JAERI-M
82-130

A BENCHMARK EXPERIMENT ON D-T NEUTRONS AND SECONDARY GAMMA RAYS STREAMING THROUGH A CONCRETE BENT DUCT

September 1982

Shun-ichi TANAKA, Yukio OYAMA, Nobuo SASAMOTO
and
Tomoo NAKAMURA

日本原子力研究所
Japan Atomic Energy Research Institute

JAERI-Mレポートは，日本原子力研究所が不定期に公刊している研究報告書です。
入手の問合わせは，日本原子力研究所技術情報部情報資料課（〒319-11茨城県那珂郡東海村）あて，お申しこしください。なお，このほかに財団法人原子力弘済会資料センター（〒319-11 茨城県那珂郡東海村日本原子力研究所内）で複写による実費頒布をおこなっております。

JAERI-M reports are issued irregularly.
Inquiries about availability of the reports should be addressed to Information Section Division of Technical Information, Japan Atomic Energy Research Institute, Tokai-mura, Naka-gun Ibaraki-ken 319-11, Japan.

編集兼発行　日本原子力研究所
印　　刷　(株)原子力資料サービス

JAERI-M 82-130

A Benchmark Experiment on D-T Neutrons and Secondary Gamma Rays Streaming through a Concrete Bent Duct

Shun-ichi TANAKA, Yukio OYAMA, Nobuo SASAMOTO
and
Tomoo NAKAMURA

Division of Reactor Engineering
Tokai Research Establishment, JAERI
(Received August 23 , 1982)

A streaming experiment was carried out to examine the behavior of D-T neutrons and secondary gamma rays in a concrete bent duct constructed as a personnel access way in the Fusion Neutronics Source Facility (FNS). The distributions in the duct were measured for neutron and gamma-ray dose equivalents, fast neutron dose, and thermal neutron flux. The energy spectra of fast neutrons and gamma rays were also measured at four positions in the duct.

This report describes in detail the experimental technique, the measured data as well as the experimental conditions such as the configuration and the composition of the structural materials and the source conditions which are essential for the analysis of the measurements.

Keywords : Streaming Benchmark Experiment, D-T Neutrons, Secondary Gamma Rays, Concrete Bent Duct, Fast Neutron Spectrum, Neutron Dose Equivalent, Fast Neutron Dose, Thermal Neutron Flux, Gamma-ray Spectrum, Exposure Dose, NE213 Detector, Rem Counter , Spectrum Weighting Technique, TLD

D-T中性子および二次ガンマ線のコンクリート迷路ストリーミングベンチマーク実験

日本原子力研究所東海研究所原子炉工学部
田中俊一・大山幸夫・笹本宣雄・中村知夫

（1982年8月23日受理）

核融合炉物理用中性子源（FNS）建家に設けられているコンクリート製の迷路を用いて，屈曲迷路内のD-T中性子とそれによって生じる二次ガンマ線の挙動を把握するためのストリーミング実験が行われた。実験では迷路内における中性子，ガンマ線の線量率分布，速中性子に対する線量率分布，熱中性子束分布が詳細に測定された。また，迷路内の4ケ所で，速中性子エネルギスペクトル，ガンマ線エネルギスペクトルも測定された。本報告書にはこれらの測定値の他，実験方法，構造物の幾何学的配置と組成，および線源条件など測定値の解析に必要なすべてのデータがまとめられている。

CONTENTS

目　　次

1. Introduction

In a Tokamak type fusion reactor, many types of openings in blanket and shield are required. The radiation streaming through the openings may cause undesirable radiation damage and radiation heating in the superconducting magnet and other components surrounding the plasma region. In particular the fast neutrons and the secondary gamma rays induced by neutrons from such large scale openings as the Neutral Beam Injector (NBI) port and the evacuation duct of cryopump can bring difficulties for the reactor design. Hence it is important to have a reliable data and method by which the streaming radiations will be evaluated accurately. However the present status of the calculations for the radiation streaming from complicated geometries is far from the accuracy required by the designer of fusion reactor, and it is necessary to have such benchmark experiments that the nuclear data and method for the design can be verified. A streaming experiment on D-T neutrons and secondary gamma rays was carried out at the personnel access way in the Fusion Neutronics Source Facility (FNS) of the JAERI. In this experiment the fast neutron and gamma-ray energy spectra in the access way were measured by applying a spectral unfolding method using a NE213 scintillation detector. The distributions of total neutron dose equivalents, fast neutron dose equivalents, thermal neutron flux, and gamma-ray exposure dose were also measured using a rem counter, a spectrum weighting function technique with a NE213 detector, and thermoluminescent dosimeters (TLDs). The angular distributions of neutrons and gamma rays emitted from the tritium target assembly were measured to obtain the accurate source conditions. The details of the experimental conditions of the configuration, the composition of the structural materials, and the detector system and responses are described in chapter 2 and 3. The results of the measurements are given in chapter 4.

2. Experimental Conditions

2.1 Experimental Configuration

The passage way used for the present experiment is an access way to the experimental room (named first target room) of FNS. A horizontal view of this target room is shwon in Fig. 1, and the vertical plans at AA' and BB' cross sections in Fig. 1 are shown in Figs. 2 and 3, respectively. The access way allows personnels to enter the 1st target room from the accelerator room. A temporary polyethylene wall of 30 cm thickness and 200 cm in height was placed at the exit of the access way in the accelerator room to shield the stray neutrons which may be produced mainly by the self-bombarding reactions of D^+ ions along the drift tube. It also define the geometrical boundary condition in this experiment. The details around the access way is given in Fig. 4. The neutrons from the tritium target which is placed at the height of 180 cm above the grating floor, impinge the access way with an angle of about 135 degree to the D^+ beam direction. Then the neutrons travel through the 96 cm × 200 cm rectangular access way and may produce the secondary gamma rays on the way. The access way and the 1st target room are constructed with an ordinary concrete of which the surface was finished by 2 cm thickness of mortar. The floor of the target room is mainly composed of an iron grating, and partly by iron board of 1 cm thickness. The atomic densities of nuclides included in these structural materials are summarized in Table 1.

The measurements of neutrons and gamma rays were performed along the paths in the access way shown as A, B and C in Fig. 5, and the positions of measured values given later are represented as the distance from the origin which is assumed at the entrance of the access way.

2.2 Source Conditions

The FNS accelerates D^+ ions to the maximum kinetic energy of 400 keV and bombared a tritium target to produce 14 MeV neutrons. The neutron yield of up to 5×10^{11} neutrons/sec can be obtained for maximum beam current of 2 mA at the 1st target position. In the present experiment, D^+ ion beam energy was 330 keV and the current at the target was varied from 5 to 400 μA to obtain an optimum condition for the measurements. Fig. 6 shows the water-cooled type tritium target assembly used

for the experiments. The amount of 25 Ci tritium is absorbed in the titanium layer evaporated on a copper backing metal by 8.1 mg/cm^2 thickness.

The neutron yield due to the $^3T(D,n)^4He$ reactions was determined by the associated particle method using a solid state alpha detector placed at the opposite angle (=180°) to the incident direction of D^+ ions within the target assembly housing. This alpha detector was also utilized as a neutron monitor throughout the experiments along with a Th-fission counter.

The $^3T(D,n)^4He$ reaction is almost isotropic in the center of mass system for low deuteron energy. The anisotropy is not negligible to the deuteron energy of 330 keV in the laboratory system. The energy and angular distribution of source neutrons are also affected by the energy spread of bombarding deuterons due to the energy loss in the titanium layer before reacting with tritium nuclei. An estimation based on Benveniste's paper[1] gave a mean reaction energy of about 160 keV for deuterons under the present condition. Furthermore, the source neutrons suffers the effects of scattering and sbsorption due to the structure of the target assembly. An energy spectrum of source neutrons emitted to the direction of $\theta = 0°$ measured by using a 2" diam. x 2" height NE213 detector is shown in Fig. 7 (see also Table 2). Similar measurements were made over the angle from 0° to 150° at the radial position of 769 cm or 600 cm from the tritium target. The angular distribution of neutron intensity was obtained as shown in Fig. 8 by the summation of the neutron flux above 12 MeV in the unfolded spectrum, which was normalized to the one at $\theta = 0°$. The error of the measurements means the upper and lower limits of the summation of the neutron flux calculated from the unfolded spectrum. Theoretically predicted cruves for the deuteron energies of 150 keV and 200 keV are also given in Fig. 8. In Fig. 9 the theoretical angular dependences of neutron energy are shown for 150 keV and 200 keV deuteron energies, respectively. The neutron energies measured at $\theta = 0°$ and $\theta = 145°$ were about 15 MeV and 13.3 MeV, respectively, lying between the two curves. From these facts, it may be resonable to conclude the mean reaction energy of deuterons to be about 160 keV, while the discrepancy between 30° and 90° in the angular distributions in Fig. 8 is regarded as the results of the interactions with the structural materials of target assembly shown in Fig. 6.

The interactions of neutrons with target assembly may produce the

secondary gamma rays at the target. The gamma-ray energy spectrum from the target in Fig. 10 (see also Table 3) was measured using the same NE213 detector as that of neutrons. Although the source region for gamma rays is not defined clearly, the result in Fig. 10 was estimated assuming that the gamma rays are produced at the same region as that of neutrons. The angular distribution of gamma-ray intensity from 0° to 105° are shown in Fig. 11, where the intensity is the sum of the photon flux above 1 MeV in the unfolded spectrum and is normalized to that at $\theta = 0°$. The spectrum shapes of gamma rays measured at different angles resemble closely to each other, and hence it is supposed that the gamma rays are emitted isotropically from the target.

3. Measurement Techniques

In this experiment a NE213 detector, a rem counter and themmoluminescent dosimeters (TLDs) were used for the neutron and gamma-ray measurements. The NE213 detector was utilized for measuring the energy spectrum of fast neutrons and gamma rays in the access way and from the tritium target as described in the previous section. The NE213 detector is a liquid scintillator packed in a glass case of 2" diam. x 2" height and has a intrinsic region of 4.65 cm diam. x 4.80 cm height of which the size is same as that used by Ingersoll et al.[2,3] The energy responses to neutrons and gamma rays in the FORIST library[4] produced by them were used for the unfolding of the pulse height distribution of the NE213 detector. Our NE213 scintillator is mounted on an RCA-6810A photomultiplier tube, and the pulses from neutrons and gamma rays after the delay line amplifier (ORTEC 460) are seperated using a rise time to height converter (JAERI 154A), and each pulses are seperately stored in a multi-channel pulse height analyzer. The block diagram of the NE213 detector system is shown in Fig. 12, and a rise time spectrum to the mixed radiations from the target are also shown in Fig. 13. The pulse height data of the multi-channel pulse height analyzer was converted to the data in Na unit defined by Verbinski et al.[5] to conform to the unit of the FORIST library. In this work, a few kinds of monoenergetic gamma rays were utilized for the calibration to assure an accuracy of 1 - 2%. In Table 4 the relationship is presented between the Na light unit values and the Compton peak and its half-maximum in the pulse height distribution of NE213 detector for each gamma rays. The energy spectrum was unfolded using the FORIST code and the library of neutron and gamma-ray response matrix from the converted pulse height data.

The neutron dose equivalent was measured using a Studsvik 2202D neutron dosimeter (so called rem counter). The dosimeter is so designed that the energy response to neutrons is approximately proportional to the neutron flux to dose conversion factor recommended by ICRP[6] to obtain the neutron dose equivalent from the neutron flux. The response of the rem counter is compared with the '71 ICRP and '77 ANSI/ANS[7] recommendations in Fig. 14 (also see Table 5). Although these are fairly consistent with each other, large differences are observed in some energy regions, especially around the 14 MeV energy. One must be

careful in the comparison of the measured data by the rem counter with the calculated neutron dose. The absolute calibration of the rem counter was carried out using a Am-Be neutron source. The neutrons of 3 - 5 MeV occupying main part of the Am-Be source spectrum are suitable to calibrate the rem counter, since the response in this energy region is in good agreement with the ICRP and ANSI/ANS recommendations as seen in Fig. 14. A sensitivity of 1 mrem/hr per 3.8 cps obtained for the present rem counter.

The neutron dose to fast neutrons above 2 MeV was also measured by the spectrum weighting function technique[8] utilizing the NE213 detector described previously. Table 6 shows the energy responses of the data measured using this technique for two different bias levels. In Fig. 15 they are compared with the ANSI/ANS recommendation. The formers are slightly lower than the latter over the whole energy region, since the function to convert the measured pulse height data to dose equivalent in the spectrum weighting function technique has been determined for lower bias level than the one used in the present measurements. The bias level has been set beweent 0.225 and 0.300 Na light unit through the present experiments, hence the fast neutron dose means a pseudo-dose equivalent measured by a dosimeter having the energy response given in Table 6.

Thermal neutron flux was measured using a pair of ^{6}LiF and ^{7}LiF TLDs.[9] The TLDs are a glass ampoule type of 2 mm diam. x 10 mm length in which 25 - 30 mg thermoluminescent powder is contained. After the TLDs are annealed at 400°C for 30 min., a pair of ^{6}LiF and ^{7}LiF TLDs covered with Cd and with thin aluminum cases was irradiated at each position to be measured. The thermoluminescence was read using a NATIONAL UD-505A TLD reader after being cooled at room temperature for one day to avoid the initial fading of the thermoluminescence. The factor to convert from the thermoluminescence to thermal neutron flux was determined by irradiating the TLDs in a standard field of thermal neutron constructed with a graphite pile, where the intensity of thermal neutrons has been determined by the Au foil measurement.

The exposure dose to gamma rays was measured using the UD-200S TLD developed by Matsushita Electric Co. Ltd. This is a $CaSO_4$(Tm) TLD covered with such a gamma-ray filter that the energy response to gamma rays is proportional to that of air from 30 keV to 10 MeV as seen in Fig. 16. In the case of UD-200S TLD the preannealing was made at 400°C

for 2 - 3 min. The calibration factor to obtain the exposure dose from the thermoluminescence was determined by an irradiation in ^{60}Co gamma-ray field, of which the source intensity has been known with an accuracy of 1 - 2%.

4. Experimental Results

4.1 Neutrons

The fast neutron spectra measured at the height of 100 cm from the floor level are represented in Table 7(1) - 7(4) for the four positions along the A-line shown in Fig. 5. In these tables ϕ_ℓ and ϕ_u show the upper and lower limits of the reliable range of the flux calculated by the FORIST code. In Fig. 17 these spectra are compared with one another, in which the distance is measured from the duct entrance defined in Fig. 5 previously. The direct neutrons of about 13.5 MeV from the tritium target are dominant at 0 cm, but at two positions of 125 cm and 255 cm in the 1st leg of the access way, the broad peaks of 12 - 12.5 MeV are distinctly observed instead of the direct neutrons. These peaks may be attributed by the single scattered neutrons with oxygen and silicon nuclides which are major components of the concrete wall. No distinct peak is observed in the spectrum at the 465 cm, and the spectrum varies drastically from the others, since only multiple scattered neutrons can reach to the position.

The distribution of the neutron dose equivalent in the access way is shown in Fig. 18 (and Table 8) with the statistical error of the counts, which was measured using a rem counter at the height of 100 cm along the A-line. The neutron dose equivalent decreases by a factor of about 20 in the 1st leg, and by a factor of about 40 in the 2nd leg.

In Table 9 the fast neutron dose distributions obtained using the spectrum weighting function technique are given. The error is caused that the measured values were obtained using two different spectrum weighting functions given in Table 6. In order to investigate the detailed behavior of the fast neutrons in the access way, dose distributions were measured along the lines A, B, and C with varying detector height. Although the values at 180 cm are slightly lower than that at 100 cm, no remarkable difference is observed in Fig. 19. In Fig. 20 an apparent discrepancy is seen between B-line's and C-line's data, but they are almost agreed with each other when they are compared at a cross section perpendicular to the duct. It is thought that the fast neutrons may travel with an uniform distribution to the forward direction of the access way. The fast neutron dose at the 0 cm is nearly equal to the neutron dose equivalent by the rem counter, but the difference increases with the distance from the entrance, and becomes as

large as the factor of 7.6 at the exit of the access way. This is caused by the fact that the neutrons scattered below the NE213 bias level contribute to the total neutron dose equivalent, and increases gradually with the distance.

Table 10 (and Fig. 21) shows the distribution of thermal neutron flux below the Cd cut off energy measured by ^{6}LiF TLD. Thermal neutrons increase once on the way, and then attenuate more slowly than the total neutron dose equivalent. A pair of ^{6}LiF TLDs was used for the measurements at each position. The error is the difference of the values measured by the TLDs.

4.2 Gamma Rays

The gamma-ray spectra at the same positions with the fast neutron spectra were also measured. The results are given in Table 11(1) - 11(4), and compared in Fig. 22. It is interesting that the spectrum profile at the every position looks almost identical. As energy resolution to gamma rays of the NE213 detector used for the spectrum measurements is not sufficient for knowing the detail of the spectrum shape, an additional measurement using a 3" diam. x 3" height NaI(Tℓ) scintillation detector was performed to clarify whether the hills around the energies of 2.1 MeV, 4.3 MeV and 6.2 MeV observed in the gamma-ray spectrum obtained by the NE213 detector represent the true full energy peaks of gamma rays or not. It was clear that the hills are not corresponding to the peaks due to monoenergetic gamma rays.

In Table 12 the distributions of the exposure dose measured by the UD-200S TLD are represented. The deviation is corresponding to the difference between the measured values by UD-200S TLDs. In Fig. 23 the distributions measured at the different detector height are compared, but any significant difference cannot be looked for the measurements. In Fig. 24 the results measured along the B and C lines are compared, and these are in a good agreement with each other when are compared on the same plane perpendicular to the duct. These results show that the gamma rays also decrease along the access way in a similar manner as that of neutrons, which is distributed uniformly on a cross sectional plane of the duct. The rate of the attenuation of the gamma-ray exposure dose through the 1st leg is almost equal to that of the neutron dose measured by the rem counter. On the other hand, the former is smaller

by a factor 2 than the latter for the 2nd leg. Consequently, the relative contribution of the gamma-ray dose to the total dose increases with the distance in the access way.

5. Concluding Remarks

Using the personnel access way in FNS, a streaming benchmark experiment was performed to examine the behavior of the D-T neutrons and the secondary gamma rays induced by the neutrons. In the present work the detailed conditions to be essential for the analysis of the measured results have been presented in addition to the measured values of the streaming neutrons and gamma rays. It is expected that these work will be applicable to the verifications of the nuclear data and the analysis codes used for estimating the streaming radiations through the blanket and shield of a D-T fusion reactor. Furthermore the experimental results of the neutron dose equivalent and the gamma-ray exposure dose present valuable informations for deriving an empirical formula of the D-T neutron streaming through a large scale concrete duct.

Acknowledgements

We would like to thank Drs. H. Maekawa and Y. Ikeda for their help of the absolute measurements of the source neutron. The authors are also grateful to Messrs. J. Kusano, C. Kutsukake, and S. Tanaka for their operation of the FNS accelerator. And we would like to thank Drs. Y. Seki and S. Matsuura for their useful advices of this document.

5. Concluding Remarks

Using the personnel access way in FNS, a streaming benchmark experiment was performed to examine the behavior of the D-T neutrons and the secondary gamma rays induced by the neutrons. In the present work the detailed conditions to be essential for the analysis of the measured results have been presented in addition to the measured values of the streaming neutrons and gamma rays. It is expected that these work will be applicable to the verifications of the nuclear data and the analysis codes used for estimating the streaming radiations through the blanket and shield of a D-T fusion reactor. Furthermore the experimental results of the neutron dose equivalent and the gamma-ray exposure dose present valuable informations for deriving an empirical formula of the D-T neutron streaming through a large scale concrete duct.

Acknowledgements

We would like to thank Drs. H. Maekawa and Y. Ikeda for their help of the absolute measurements of the source neutron. The authors are also grateful to Messrs. J. Kusano, C. Kutsukake, and S. Tanaka for their operation of the FNS accelerator. And we would like to thank Drs. Y. Seki and S. Matsuura for their useful advices of this document.

References

1) Benveniste J. and Zenger J. : "Information on the Reaction Produced in the $^{3}H(d,n)^{4}He$", UCRL-4266 (1954)
2) Ingersoll D.T., Wehring B.W. and Johnson R.H. : "Neutron Response Matrix for Unfolding NE213 Measurements to 21 MeV", Proc. of a Seminar Workshop on A REVIEW OF RADIATION ENERGY SPECTRA UNFOLDING, ORNL/RSIC-40, 47 (1976)
3) Ingersoll D.T. and Wehring B.W. : Nucl. Instr. Meth., 147, 551 (1977)
4) FORIST spectra unfolding Code, Radiation Shielding Information Center, ORNL, PSR-92 (1975)
5) Verbinski V.V. and Burrus W.R. : Nucl. Instr. Meth., 65, 8 (1968)
6) ICRP(1971) : Appendix to Revision of Publication 3 and 4
7) American National Standard : "Neutron and Gamma-ray Flux to Dose Rate Factors", ANSI/ANS-6.1.1 (1977)
8) Oyama Y. and Tanaka S. : "Neutron Dosimetry Based on the Spectrum Weighting Function Method Using a NE213 Scintillation Detector", JAERI-M 9982 (1982)
9) Tanaka S. and Furuta Y. : Nucl. Instr. Meth., 133, 495 (1976)

Table 1 Atomic densities of the structural materials of the 1st target room and of the personnel access way

Element	Ordinary Concrete[¢]	Mortar[¢¢]	Grating	Polyethylene	Air
H	7.94-3[$] (1.01-2)[$$]	1.82-2[#]		7.91-2	
C	5.41-4			3.96-2	
N					4.20-5
O	4.32-2	4.22-2			1.13-5
Na	7.86-4	7.16-4			
Mg	3.82-4	1.94-4			
Al	2.64-3	2.00-3			
Si	1.48-2	1.26-2			
S	5.15-5	6.52-5			
K	5.29-4	4.71-4			
Ca	2.56-3	3.59-3			
Fe	5.86-4	2.78-4	8.48-2		

read as 1.82×10^{-2}
¢¢ the chemical analysis for a typical mortar by Hitachi Cement Co. Ltd
¢ the average of the chemical analysis for several samples of ordinary concrete used in FNS
$ the value excluding the free water component
$$ the value including the free water component

Table 2 Energy spectrum of the source neutrons emitted from the tritium target to the direction of $\theta = 0°$

Energy (MeV)	Neutron Intensity$^{\$}$ (n MeV^{-1}ster^{-1} /source n)	Energy (MeV)	Neutron Intensity (n MeV^{-1}ster^{-1} /source n)	Energy (MeV)	Neutron Intensity (n MeV^{-1}ster^{-1} /source n)
2.2	2.62-04$^{\#}$	7.0	4.93-04	11.8	0.0
2.4	1.23-03	7.2	2.89	12.0	0.0
2.6	1.72	7.4	1.47	12.2	0.0
2.8	1.99	7.6	9.73-05	12.4	0.0
3.0	2.41	7.8	1.28-04	12.6	1.77-04
3.2	2.87	8.0	2.05	12.8	6.49
3.4	2.92	8.2	2.89	13.0	1.42-03
3.6	2.43	8.4	3.56	13.2	2.70
3.8	1.75	8.6	3.90	13.4	4.76
4.0	1.24	8.8	3.85	13.6	7.83
4.2	1.00	9.0	3.44	13.8	1.22-02
4.4	9.39-04	9.2	2.78	14.0	1.81
4.6	9.65	9.4	2.00	14.2	2.53
4.8	1.02-03	9.6	1.19	14.4	3.31
5.0	1.06	9.8	3.23-05	14.6	4.03
5.2	1.05	10.0	0.0	14.8	4.54
5.4	9.65-04	10.2	0.0	15.0	4.71
5.6	8.56	10.4	0.0	15.2	4.41
5.8	7.96	10.6	0.0	15.4	3.78
6.0	8.04	10.8	0.0	15.6	2.94
6.2	8.61	11.0	0.0	15.8	2.08
6.4	8.91	11.2	0.0	16.0	1.34
6.6	8.43	11.4	0.0	16.2	8.43-03
6.8	7.01	11.6	0.0	16.4	4.71

read as 6.06×10^{-5}

$ represent the neutron intensity emitted to the direction of $\theta = 0°$ per source neutron, of which the intensity was determined by the associated alpha-particle measurements

Table 3 Energy spectrum of the souce gamma rays emitted from the tritium target assembly to the direction of θ = 90°

Energy (MeV)	Gamma-Ray Intensity # (photon MeV^{-1} ster^{-1} /source neutron)	Energy (MeV)	Gamma-Ray Intensity (photon MeV^{-1} ster^{-1} /source neutron)	Energy (MeV)	Gamma-Ray Intensity (photon MeV^{-1} ster^{-1} /source neutron)
1.0	2.50 -02	4.5	5.25 -03	8.0	6.37 -04
1.1	2.40	4.6	4.80	8.1	5.81
1.2	2.17	4.7	4.33	8.2	5.31
1.3	2.11	4.8	3.85	8.3	4.90
1.4	1.97	4.9	3.39	8.4	4.55
1.5	1.81	5.0	2.99	8.5	4.26
1.6	1.69	5.1	2.64	8.6	4.03
1.7	1.61	5.2	2.39	8.7	3.83
1.8	1.50	5.3	2.22	8.8	3.65
1.9	1.35	5.4	2.16	8.9	3.48
2.0	1.19	5.5	2.18	9.0	3.32
2.1	1.02	5.6	2.26	9.1	3.15
2.2	8.87 -03	5.7	2.38	9.2	2.98
2.3	7.92	5.8	2.51	9.3	2.81
2.4	7.32	5.9	2.62	9.4	2.61
2.5	6.98	6.0	2.70	9.5	2.42
2.6	6.83	6.1	2.72	9.6	2.23
2.7	6.74	6.2	2.68	9.7	2.03
2.8	6.61	6.3	2.58	9.8	1.85
2.9	6.32	6.4	2.44	9.9	1.66
3.0	5.89	6.5	2.29	10.0	1.49
3.1	5.37	6.6	2.11	10.1	1.33
3.2	4.90	6.7	1.94	10.2	1.19
3.3	4.59	6.8	1.77	10.3	1.06
3.4	4.47	6.9	1.63	10.4	9.35 -05
3.5	4.57	7.0	1.49	10.5	8.30
3.6	4.80	7.1	1.37	10.6	7.34
3.7	5.13	7.2	1.28	10.7	6.52
3.8	5.47	7.3	1.17	10.8	5.82
3.9	5.79	7.4	1.09	10.9	5.21
4.0	6.03	7.5	1.01	11.0	4.68
4.1	6.14	7.6	9.19 -04		
4.2	6.11	7.7	8.46		
4.3	5.95	7.8	7.69		
4.4	5.64	7.9	7.00		

represent the gamma-ray intensity emitted to the direction of θ = 90° per source neutron

Table 4 Light unit values of the Compton peaks to monoenergetic gamma rays used for the pulse height calibration of NE213 detector

Isotope	Gamma-ray Energy (MeV)	Na Light Unit	
		Compton Peak	Half-Maximum
^{22}Na	0.511	0.237	0.294
	1.274	0.788	0.883
^{137}Cs	0.662	0.341	0.406
^{54}Mn	0.835	0.464	0.540
^{88}Y	0.898	0.490	0.581
	1.836	1.214	1.334

Table 5 Neutron flux to dose equivalent rate conversion factors

Neutron Energy	Flux to Dose Rate Conversion Factors (mrem·hr^{-1}/n·cm^{-2}·sec^{-1})		
(MeV)	ANSI/ANS	ICRP	2202D
2.5-08	3.67-03#	3.79-03	2.35-03
1.0-07	3.67	4.14	2.60
1.0-06	4.46	4.50	2.80
1.0-05	4.54	4.34	3.60
1.0-04	4.18	4.19	4.20
1.0-03	3.76	3.67	4.80
1.0-02	3.56	3.53	5.80
1.0-01	2.17-02	2.06-02	2.70-02
5.0-01	9.26	6.92	7.45
1.0	1.32-01	1.16-01	1.18-01
2.0		1.44	1.33
2.5	1.25-01		1.30
5.0	1.56	1.50-01	1.15
7.0	1.47		1.10
1.0+01	1.47	1.50-01	1.02
1.4+01	2.08		9.70-02
2.0+01	2.27	1.57-01	9.30

read as 3.67×10^{-3}

Table 6 Spectrum weighting functions with the bias levels of 0.225 and 0.300 Na light unit to obtain the fast neutron dose by using a 2" x 2" NE213 detector

Energy (MeV)	rem hr^{-1}/n cm^{-2} sec^{-1}		Energy (MeV)	rem hr^{-1}/n cm^{-2} sec^{-1}	
	0.225*	0.300*		0.225*	0.300*
1.13	2.05-07		6.78	1.37-04	1.34-04
1.21	1.68-06	2.19-10	7.04	1.37	1.34
1.31	9.30	2.41-08	7.29	1.36	1.33
1.41	1.99-05	5.98-07	7.53	1.36	1.33
1.51	3.04	4.34-06	7.78	1.35	1.33
1.61	4.04	1.28-05	8.03	1.35	1.32
1.77	5.49	2.68	8.52	1.38	1.35
1.92	6.61	4.12	9.01	1.40	1.38
2.08	7.49	5.41	9.51	1.43	1.41
2.23	8.22	6.46	10.0	1.46	1.44
2.48	9.01	7.59	10.5	1.49	1.47
2.74	9.76	8.57	11.0	1.53	1.51
2.99	1.05-04	9.44	11.5	1.58	1.55
3.24	1.11	1.02-04	12.0	1.64	1.61
3.49	1.17	1.09	12.5	1.71	1.68
3.74	1.21	1.14	13.0	1.79	1.76
3.99	1.25	1.19	13.5	1.87	1.84
4.24	1.28	1.22	14.0	1.94	1.91
4.41	1.30	1.24	14.5	1.98	1.95
4.58	1.32	1.27	15.0	2.01	1.97
4.75	1.34	1.29	16.1	2.03	2.00
4.92	1.36	1.31	16.5	2.07	2.04
5.19	1.38	1.33	16.9	2.10	2.07
5.47	1.39	1.35	17.4	2.13	2.10
5.74	1.39	1.35	17.8	2.16	2.14
6.02	1.38	1.35	18.3	2.18	2.16
6.27	1.38	1.34	18.9	2.20	2.17
6.53	1.37	1.34	19.4	2.20	2.18

* Bias level of pulse height in Na light unit

Table 7(1) Energy spectrum of fast neutrons at 0 cm from the duct inlet

Energy (MeV)	n cm^{-2}sec^{-1}MeV^{-1}/source neutron sec^{-1}		Energy (MeV)	n cm^{-2}sec^{-1}MeV^{-1}/source neutron sec^{-1}		Energy (MeV)	n cm^{-2}sec^{-1}MeV^{-1}/source neutron sec^{-1}	
	ϕ_{lower}	ϕ_{upper}		ϕ_{lower}	ϕ_{upper}		ϕ_{lower}	ϕ_{upper}
1.4	3.00 -08	3.21 -08	7.0	3.53 -09	6.79 -09	12.6	4.95 -08	5.39 -08
1.6	5.04	5.28	7.2	3.58	7.00	12.8	5.91	6.33
1.8	4.53	4.77	7.4	3.61	7.12	13.0	6.72	7.14
2.0	3.98	4.21	7.6	3.51	7.16	13.2	7.25	7.68
2.2	3.63	3.86	7.8	3.32	7.05	13.4	7.39	7.82
2.4	3.53	3.74	8.0	3.09	6.84	13.6	7.11	7.53
2.6	3.28	3.47	8.2	2.82	6.65	13,8	6.47	6.84
2.8	2.65	2.81	8.4	2.56	6.44	14.0	5.58	5.89
3.0	2.09	2.21	8.6	2.26	6.19	14.2	4.58	4.84
3.2	1.77	1.88	8.8	1.95	5.95	14.4	3.58	3.82
3.4	1.54	1.66	9.0	1.67	5.72	14.6	2.70	2.93
3.6	1.34	1.50	9.2	1.52	5.65	14.8	2.00	2.19
3.8	1.19	1.39	9.4	1.58	5.75	15.0	1.48	1.63
4.0	1.15	1.33	9.6	1.81	6.05	15.2	1.09	1.22
4.2	1.14	1.35	9.8	2.12	6.47	15.4	8.14 -09	9.21 -09
4.4	1.14	1.39	10.0	2.37	6.82	15.6	6.14	7.02
4.6	1.14	1.40	10.2	2.47	7.05	15.8	4.70	5.37
4.8	1.11	1.37	10.4	2.42	7.11	16.0	3.61	4.11
5.0	1.05	1.31	10.6	2.35	7.11	16.2	2.77	3.11
5.2	9.63 -09	1.21	10.8	2.47	7.28	16.4	2.11	2.35
5.4	8.49	1.09	11.0	3.07	7.89	16.6	1.58	1.75
5.6	7.26	9.72 -09	11.2	4.40	9.26	16.8	1.16	1.29
5.8	6.11	8.68	11.4	6.75	1.16 -08	17.0	8.39 -10	9.35 -10
6.0	5.18	7.91	11.6	1.03 -08	1.53	17.2	5.89	6.65
6.2	4.49	7.35	11.8	1.53	2.04	17.4	4.02	4.65
6.4	4.05	6.93	12.0	2.19	2.68	17.6	2.63	3.18
6.6	3.75	6.68	12.2	3.00	3.49	17.8	1.62	2.14
6.8	3.58	6.65	12.4	3.93	4.40	18.0	9.19 -11	1.41

Table 7(2) Energy spectrum of fast neutrons at 125 cm from the duct inlet

Energy (MeV)	n cm^{-2}sec^{-1}MeV^{-1}/source neutron sec^{-1}		Energy (MeV)	n cm^{-2}sec^{-1}MeV^{-1}/source neutron sec^{-1}		Energy (MeV)	n cm^{-2}sec^{-1}MeV^{-1}/source neutron sec^{-1}	
	ϕ_{lower}	ϕ_{upper}		ϕ_{lower}	ϕ_{upper}		ϕ_{lower}	ϕ_{upper}
1.4	7.84 -09	8.22 -09	7.0	7.58 -10	9.27 -10	12.6	1.72 -09	1.85 -09
1.6	1.05 -08	1.09 -08	7.2	6.86	8.59	12.8	1.57	1.69
1.8	8.99 -09	9.48 -09	7.4	6.12	7.86	13.0	1.40	1.52
2.0	7.57	8.05	7.6	5.44	7.17	13.2	1.22	1.33
2.2	7.42	7.88	7.8	4.90	6.63	13.4	1.05	1.15
2.4	6.99	7.37	8.0	4.54	6.26	13.6	8.88 -10	9.70 -10
2.6	6.17	6.53	8.2	4.36	6.07	13.8	7.41	8.10
2.8	5.47	5.80	8.4	4.32	6.02	14.0	6.10	6.68
3.0	4.89	5.16	8.6	4.38	6.06	14.2	4.98	5.44
3.2	4.00	4.25	8.8	4.49	6.16	14.4	4.01	4.40
3.4	3.31	3.52	9.0	4.62	6.26	14.6	3.21	3.52
3.6	2.99	3.16	9.2	4.70	6.35	14.8	2.54	2.78
3.8	2.74	2.89	9.4	4.74	6.38	15.0	2.00	2.19
4.0	2.46	2.59	9.6	4.75	6.40	15.2	1.57	1.70
4.2	2.14	2.30	9.8	4.81	6.44	15.4	1.22	1.32
4.4	1.90	2.06	10.0	5.04	6.65	15.6	9.37 -11	1.02
4.6	1.81	1.98	10.2	5.51	7.11	15.8	7.15	7.83 -11
4.8	1.83	1.98	10.4	6.30	7.89	16.0	5.37	5.91
5.0	1.81	1.99	10.6	7.44	9.04	16.2	3.96	4.41
5.2	1.75	1.95	10.8	8.96	1.06 -09	16.4	2.85	3.23
5.4	1.65	1.85	11.0	1.08 -09	1.23	16.6	1.99	2.33
5.6	1.53	1.72	11.2	1.27	1.44	16.8	1.35	1.65
5.8	1.40	1.57	11.4	1.48	1.64	17.0	8.64 -12	1.16
6.0	1.25	1.42	11.6	1.65	1.81	17.2	5.19	8.12 -12
6.2	1.10	1.27	11.8	1.79	1.95	17.4	2.78	5.78
6.4	9.90 -10	1.16	12.0	1.88	2.01	17.6	1.17	4.22
6.6	9.01	1.06	12.2	1.88	2.01	17.8	1.15	3.22
6.8	8.28	9.90 -10	12.4	1.83	1.95	18.0		

Table 7(3) Energy spectrum of fast neutrons at 255 cm from the duct inlet

Energy (MeV)	n cm^{-2}sec^{-1}MeV^{-1}/source neutron sec^{-1}		Energy (MeV)	n cm^{-2}sec^{-1}MeV^{-1}/source neutron sec^{-1}		Energy (MeV)	n cm^{-2}sec^{-1}MeV^{-1}/source neutron sec^{-1}	
	ϕ_{lower}	ϕ_{upper}		ϕ_{lower}	ϕ_{upper}		ϕ_{lower}	ϕ_{upper}
1.4	2.54 -09	2.66 -09	7.0	1.82 -10	2.20 -10	12.6	3.68 -10	4.09 -10
1.6	3.19	3.32	7.2	1.73	2.13	12.8	3.54	3.91
1.8	2.68	2.83	7.4	1.67	2.07	13.0	3.30	3.63
2.0	2.36	2.51	7.6	1.60	2.00	13.2	2.99	3.27
2.2	2.18	2.31	7.8	1.51	1.90	13.4	2.63	2.87
2.4	1.89	2.00	8.0	1.40	1.79	13.6	2.25	2.46
2.6	1.68	1.78	8.2	1.29	1.67	13.8	1.87	2.05
2.8	1.52	1.61	8.4	1.17	1.55	14.0	1.53	1.68
3.0	1.41	1.48	8.6	1.07	1.44	14.2	1.23	1.34
3.2	1.18	1.23	8.8	9.61 -11	1.33	14.4	9.69 -11	1.07
3.4	9.00 -10	9.48 -10	9.0	8.78	1.25	14.6	7.65	8.39 -11
3.6	7.00	7.48	9.2	8.43	1.20	14.8	6.04	6.61
3.8	5.96	6.52	9.4	8.74	1.23	15.0	4.83	5.26
4.0	5.65	6.09	9.6	9.74	1.34	15.2	3.86	4.20
4.2	5.43	5.87	9.8	1.13 -10	1.51	15.4	3.08	3.36
4.4	5.22	5.74	10.0	1.32	1.73	15.6	2.45	2.68
4.6	4.96	5.52	10.2	1.52	1.97	15.8	1.92	2.11
4.8	4.65	5.22	10.4	1.71	2.19	16.0	1.48	1.64
5.0	4.43	4.96	10.6	1.90	2.39	16.2	1.11	1.24
5.2	4.16	4.65	10.8	2.08	2.55	16.4	8.00 -12	9.30 -12
5.4	3.88	4.33	11.0	2.27	2.73	16.6	5.74	6.82
5.6	3.58	4.02	11.2	2.48	2.93	16.8	3.94	4.96
5.8	3.26	3.67	11.4	2.70	3.18	17.0	2.57	3.59
6.0	2.94	3.34	11.6	2.96	3.46	17.2	1.57	2.62
6.2	2.64	3.03	11.8	3.22	3.74	17.4	8.61 -13	1.93
6.4	2.36	2.75	12.0	3.46	3.97	17.6	3.59	1.45
6.6	2.13	2.51	12.2	3.63	4.12	17.8	1.80	1.13
6.8	1.95	2.33	12.4	3.71	4.16	18.0		

Table 7(4) Energy spectrum of fast neutrons at 465 cm from the duct inlet

Energy (MeV)	n cm^{-2}sec^{-1}MeV^{-1}/source neutron sec^{-1}		Energy (MeV)	n cm^{-2}sec^{-1}MeV^{-1}.source neutron sec^{-1}		Energy (MeV)	n cm^{-2}sec^{-1}MeV^{-1}.source neutron sec^{-1}	
	ϕ_{lower}	ϕ_{upper}		ϕ_{lower}	ϕ_{upper}		ϕ_{lower}	ϕ_{upper}
1.4	3.99 -11	4.36 -11	7.0	2.83 -12	3.83 -12	12.6	9.62 -13	1.28 -12
1.6	1.31 -10	1.36 -10	7.2	3.13	4.15	12.8	9.16	1.22
1.8	1.30	1.34	7.4	3.32	4.36	13.0	8.55	1.15
2.0	1.00	1.05	7.6	3.27	4.27	13.2	7.60	1.05
2.2	7.30 -11	7.81 -11	7.8	2.99	3.96	13.4	6.31	9.18 -13
2.4	5.59	6.03	8.0	2.62	3.55	13.6	4.80	7.63
2.6	4.78	5.19	8.2	2.29	3.18	13.8	3.36	6.10
2.8	4.34	4.73	8.4	2.11	2.97	14.0	2.14	4.71
3.0	3.89	4.24	8.6	2.14	2.92	14.2	1.26	3.57
3.2	3.41	3.73	8.8	2.32	3.06	14.4	6.61 -14	2.76
3.4	2.87	3.20	9.0	2.57	3.27	14.6	2.09	2.36
3.6	2.41	2.74	9.2	2.78	3.48	14.8		
3.8	2.01	2.34	9.4	2.90	3.59	15.0		
4.0	1.71	2.00	9.6	2.92	3.59	15.2		
4.2	1.47	1.74	9.8	3.55	3.50	15.4		
4.4	1.28	1.53	10.0	2.78	3.41	15.6		
4.6	1.15	1.38	10.2	2.74	3.34	15.8		
4.8	1.06	1.26	10.4	2.78	3.32	16.0		
5.0	9.81 -12	1.16	10.6	2.87	3.36	16.2		
5.2	8.93	1.05	10.8	2.97	3.43	16.4		
5.4	7.91	9.37 -12	11.0	2.99	3.48	16.6		
5.6	6.86	8.18	11.2	2.87	3.38	16.8		
5.8	5.91	7.09	11.4	2.62	3.15	17.0		
6.0	5.01	6.14	11.6	2.24	2.76	17.2		
6.2	4.10	5.24	11.8	1.83	2.30	17.4		
6.4	3.29	4.43	12.0	1.46	1.88	17.6		
6.6	2.76	3.80	12.2	1.20	1.56	17.8		
6.8	2.64	3.62	12.4	1.04	1.37	18.0		

Table 8 Distribution of neutron dose equivalents in the access way measured by a Studsvik neutron dosimeter

Distance from Duct Inlet (cm)	Measured Value (mrem hr^{-1}/source neutron sec^{-1})
-100	4.65 -08
- 50	4.54
0	3.94
50	1.80
100	8.55 -09
150	4.99
200	3.04
256	2.19(±0.04)-09
316	1.01(±0.02)
366	3.55(±0.13)-10
416	1.87(±0.05)
460	1.04(±0.04)
515	5.48(±0.28)-11
A^- 565	3.51(±0.22)
A^+ "	4.51(±0.16)
615	1.28(±0.01)

Table 10 Distribution of thermal neutron flux in the access way measured by ^6LiF TLD

Distance from Duct Inlet (cm)	Thermal Neutron Flux (n cm^{-2} sec^{-1}/source neutron sec^{-1})
0	3.61(±0.36)-08*
50	7.85(±0.79)
100	9.80(±0.95)
150	1.21(±0.095)-07
200	8.61(±0.99)-08
256	7.22(±0.89)
316	2.80(±0.26)
366	1.66(±0.23)
416	9.43(±1.73)-09
460	5.88(±1.54)

* read as $3.61(\pm 0.36) \times 10^{-8}$

Table 9 Distributions of fast neutron dose in the access way measured using the spectrum weighting function technique

Distance from Duct Inlet (cm)	Fast Neutron Dose Rate (rem hr^{-1}/source neutron sec^{-1}) A-line *100 cm	A-line *180 cm	B-line	C-line
-100	5.01(±0.21)-11**	5.41(±0.14)-11	4.49(±0.13)-11	5.57(±0.15)-11
- 50	4.70(±0.13)	4.75(±0.13)		
0	4.37(±0.11)	4.42(±0.11)	4.17(±0.11)	4.97(±0.13)
25	4.08(±0.10)			
50		1.10(±0.07)		
75	5.62(±0.31)-12			
100		3.01(±0.19)-12	4.52(±0.25)-12	2.96(±0.19)-12
125	2.97(±0.18)			
150		1.74(±0.11)		
175	1.58(±0.10)			
200		1.03(±0.06)		
208			8.87(±0.60)-13	1.13(±0.07)
228			6.55(±0.44)	
256	6.36(±0.43)-13	6.47(±0.44)-13		
295				6.26(±0.43)-13
309			3.18(±0.39)-14	
315	5.30(±0.39)	3.39(±0.30)		
365	6.64(±0.69)-14	3.06(±0.58)-14		
384			1.43(±0.17)	3.97(±0.31)
415	2.95(±0.32)	2.66(±0.29)		
465	1.75(±0.18)	1.41(±0.16)		
471				5.62(±0.57)-14
520	8.27(±0.99)-15	8.14(±0.81)-15		
546				1.63(±0.18)
A^{+}_{-}570	7.22(±0.76)			
A^{-}_{+}570	7.81(±0.77)			
A^{+}_{-}620	1.61(±0.19)			
A^{-}_{+}620	1.15(±0.14)			

* Detector height

** Read as $5.01(\pm 0.21) \times 10^{-11}$

Table 11(1) Gamma-ray energy spectrum at 0 cm from the duct inlet

Energy (MeV)	photons $cm^{-2}sec^{-1}MeV^{-1}$/source n sec^{-1}		Energy (MeV)	photons $cm^{-2}sec^{-1}MeV^{-1}$/source n sec^{-1}		Energy (MeV)	photons $cm^{-2}sec^{-1}MeV^{-1}$/source n sec^{-1}	
	ϕ_{lower}	ϕ_{upper}		ϕ_{lower}	ϕ_{upper}		ϕ_{lower}	ϕ_{upper}
1.0			3.7	2.44 -08	3.51 -08	6.4	1.38 -08	1.74 -08
1.1			3.8	2.68	3.72	6.5	1.32	1.65
1.2			3.9	2.93	3.93	6.6	1.25	1.56
1.3			4.0	3.09	4.10	6.7	1.18	1.47
1.4	9.09 -08	1.33 -07	4.1	3.16	4.19	6.8	1.10	1.39
1.5	8.70	1.45	4.2	3.14	4.17	6.9	1.02	1.30
1.6	9.00	1.30	4.3	3.07	4.02	7.0	9.42 -09	1.22
1.7	8.88	1.15	4.4	2.93	3.79	7.1	8.75	1.14
1.8	8.30	9.37 -08	4.5	2.77	3.49	7.2	8.12	1.07
1.9	5.82	8.45	4.6	2.58	3.19	7.3	7.54	9.95 -09
2.0	3.42	7.86	4.7	2.47	2.95	7.4	7.02	9.24
2.1	2.26	7.30	4.8	2.17	2.72	7.5	6.49	8.58
2.2	2.28	6.81	4.9	2.00	2.54	7.6	6.00	7.93
2.3	2.84	6.40	5.0	1.84	2.39	7.7	5.53	7.33
2.4	3.39	6.09	5.1	1.73	2.26	7.8	5.07	6.75
2.5	3.70	5.81	5.2	1.64	2.16	7.9	4.65	6.21
2.6	3.84	5.45	5.3	1.58	2.07	8.0	4.26	5.70
2.7	3.70	5.12	5.4	1.56	2.00	8.1	3.91	5.24
2.8	3.33	4.86	5.5	1.55	1.95	8.2	3.61	4.81
2.9	2.96	4.56	5.6	1.56	1.91	8.3	3.33	4.42
3.0	2.75	4.12	5.7	1.57	1.89	8.4	3.10	4.07
3.1	2.65	3.67	5.8	1.57	1.89	8.5	2.91	3.74
3.2	2.46	3.39	5.9	1.56	1.91	8.6	2.74	3.46
3.3	2.23	3.26	6.0	1.53	1.91	8.7	2.56	3.19
3.4	2.09	3.19	6.1	1.51	1.89	8.8	2.42	2.96
3.5	2.10	3.21	6.2	1.47	1.86	8.9	2.26	2.77
3.6	2.23	3.32	6.3	1.43	1.81	9.0	2.10	2.60

Table 11(2) Gamma-ray energy spectrum at 125 cm from the duct inlet

Energy (MeV)	photons $cm^{-2} sec^{-1} MeV^{-1}$/source n sec^{-1}		Energy (MeV)	photons $cm^{-2} sec^{-1} MeV^{-1}$/source n sec^{-1}		Energy (MeV)	photons $cm^{-2} sec^{-1} MeV^{-1}$/source n sec^{-1}	
	ϕ_{lower}	ϕ_{upper}		ϕ_{lower}	ϕ_{upper}		ϕ_{lower}	ϕ_{upper}
1.0			3.7	4.76 -09	6.26 -09	6.4	3.70 -09	4.29 -09
1.1			3.8	5.45	7.00	6.5	3.60	4.16
1.2			3.9	6.18	7.74	6.6	3.49	4.00
1.3			4.0	6.84	8.39	6.7	3.35	3.85
1.4	1.63 -08	2.33 -08	4.1	7.35	8.88	6.8	3.21	3.71
1.5	1.41	2.39	4.2	7.66	9.15	6.9	3.07	3.57
1.6	1.61	2.19	4.3	7.75	9.18	7.0	2.93	3.45
1.7	1.84	2.19	4.4	7.64	8.96	7.1	2.81	3.33
1.8	2.05	2.19	4.5	7.35	8.56	7.2	2.69	3.21
1.9	1.98	2.37	4.6	6.93	8.01	7.3	2.57	3.08
2.0	1.81	2.46	4.7	6.43	7.39	7.4	2.46	2.94
2.1	1.64	2.37	4.8	5.88	6.76	7.5	2.33	2.80
2.2	1.48	2.12	4.9	5.30	6.17	7.6	2.20	2.65
2.3	1.32	1.80	5.0	4.76	5.63	7.7	2.06	2.50
2.4	1.18	1.51	5.1	4.28	5.17	7.8	1.91	2.33
2.5	1.06	1.29	5.2	3.89	4.79	7.9	1.77	2.16
2.6	1.02	1.17	5.3	3.62	4.50	8.0	1.62	1.99
2.7	1.01	1.14	5.4	3.47	4.29	8.1	1.49	1.83
2.8	9.81 -09	1.15	5.5	3.41	4.17	8.2	1.35	1.67
2.9	9.29	1.11	5.6	3.44	4.14	8.3	1.22	1.52
3.0	8.37	9.91 -09	5.7	3.52	4.17	8.4	1.12	1.37
3.1	7.17	8.31	5.8	3.60	4.25	8.5	1.02	1.24
3.2	5.83	6.88	5.9	3.68	4.36	8.6	9.29 -10	1.13
3.3	4.71	5.88	6.0	3.74	4.46	8.7	8.51	1.02
3.4	4.07	5.37	6.1	3.78	4.50	8.8	7.81	9.21 -10
3.5	3.95	5.31	6.2	3.79	4.49	8.9	7.18	8.35
3.6	4.22	5.65	6.3	3.76	4.41	9.0	6.60	7.59

Table 11(3) Gamma-ray energy spectrum at 255 cm from the duct inlet

Energy (MeV)	photons $cm^{-2}sec^{-1}MeV^{-1}$/source n sec^{-1}		Energy (MeV)	photons $cm^{-2}sec^{-1}MeV^{-1}$/source n sec^{-1}		Energy (MeV)	photons $cm^{-2}sec^{-1}MeV^{-1}$/source n sec^{-1}	
	ϕ_{lower}	ϕ_{upper}		ϕ_{lower}	ϕ_{upper}		ϕ_{lower}	ϕ_{upper}
1.0			3.7	1.46 -09	2.21 -09	6.4	1.33 -09	1.59 -09
1.1			3.8	1.63	2.37	6.5	1.27	1.52
1.2			3.9	1.82	2.54	6.6	1.20	1.44
1.3	1.70 -09	1.81 -08	4.0	2.00	2.73	6.7	1.13	1.36
1.4	4.97	7.66 -09	4.1	2.16	2.90	6.8	1.05	1.28
1.5	4.20	7.82	4.2	2.29	3.03	6.9	9.81 -10	1.21
1.6	5.11	7.33	4.3	2.39	3.10	7.0	9.17	1.14
1.7	5.82	7.17	4.4	2.46	3.09	7.1	8.57	1.07
1.8	6.58	7.22	4.5	2.46	3.02	7.2	8.03	1.01
1.9	6.36	8.03	4.6	2.40	2.87	7.3	7.55	9.54 -10
2.0	5.98	8.73	4.7	2.28	2.71	7.4	7.12	8.95
2.1	5.72	8.73	4.8	2.10	2.50	7.5	6.69	8.47
2.2	5.50	8.14	4.9	1.89	2.28	7.6	6.31	7.98
2.3	5.06	7.01	5.0	1.68	2.05	7.7	5.77	7.49
2.4	4.41	5.77	5.1	1.47	1.83	7.8	5.50	7.01
2.5	3.71	4.77	5.2	1.30	1.66	7.9	5.15	6.58
2.6	3.22	4.07	5.3	1.18	1.52	8.0	4.81	6.15
2.7	2.88	3.71	5.4	1.11	1.43	8.1	4.50	5.77
2.8	2.56	3.60	5.5	1.09	1.39	8.2	4.21	5.37
2.9	2.33	3.41	5.6	1.12	1.40	8.3	3.94	5.00
3.0	2.16	3.06	5.7	1.18	1.43	8.4	3.70	4.64
3.1	1.99	2.63	5.8	1.25	1.50	8.5	3.48	4.31
3.2	1.77	2.30	5.9	1.30	1.57	8.6	3.27	3.98
3.3	1.52	2.12	6.0	1.35	1.63	8.7	3.07	3.68
3.4	1.35	2.03	6.1	1.38	1.66	8.8	2.87	3.39
3.5	1.30	2.03	6.2	1.39	1.67	8.9	2.69	3.12
3.6	1.34	2.09	6.3	1.36	1.64	9.0	2.49	2.86

Table 11(4) Gamma-ray energy spectrum at 465 cm from the duct inlet

Energy (MeV)	photons $cm^{-2}sec^{-1}MeV^{-1}$/source n sec^{-1}		Energy (MeV)	photons $cm^{-2}sec^{-1}MeV^{-1}$/source n sec^{-1}		Energy (MeV)	photons $cm^{-2}sec^{-1}MeV^{-1}$/source n sec^{-1}	
	ϕ_{lower}	ϕ_{upper}		ϕ_{lower}	ϕ_{upper}		ϕ_{lower}	ϕ_{upper}
1.0			3.7	1.74 -10	2.90 -10	6.4	1.42 -10	1.91 -10
1.1			3.8	1.99	3.16	6.5	1.32	1.78
1.2			3.9	2.24	3.36	6.6	1.20	1.63
1.3			4.0	2.44	3.56	6.7	1.08	1.50
1.4	5.57 -10	9.52 -10	4.1	2.60	3.72	6.8	9.75 -11	1.38
1.5	4.12	9.54	4.2	2.70	3.79	6.9	8.85	1.29
1.6	4.48	8.73	4.3	2.75	3.77	7.0	8.22	1.22
1.7	5.42	8.35	4.4	2.72	3.66	7.1	7.79	1.16
1.8	7.00	8.14	4.5	2.65	3.49	7.2	7.53	1.12
1.9	7.00	9.95	4.6	2.51	3.26	7.3	7.40	1.09
2.0	6.79	1.18 -09	4.7	2.30	3.00	7.4	7.33	1.06
2.1	6.92	1.25	4.8	2.05	2.75	7.5	7.25	1.03
2.2	7.07	1.20	4.9	1.78	2.47	7.6	7.15	1.01
2.3	6.87	1.06	5.0	1.51	2.22	7.7	7.02	9.75 -11
2.4	6.11	8.93 -10	5.1	1.28	1.99	7.8	6.84	9.41
2.5	5.06	7.23	5.2	1.11	1.81	7.9	6.62	9.03
2.6	4.10	5.75	5.3	1.02	1.68	8.0	6.36	8.63
2.7	3.28	4.71	5.4	1.00	1.62	8.1	6.11	8.19
2.8	2.62	4.17	5.5	1.05	1.62	8.2	5.83	7.76
2.9	2.22	3.82	5.6	1.66	1.68	8.3	5.55	7.30
3.0	2.02	3.38	5.7	1.28	1.77	8.4	5.29	6.84
3.1	1.87	2.90	5.8	1.41	1.90	8.5	5.04	6.41
3.2	1.63	2.57	5.9	1.50	2.01	8.6	4.78	5.98
3.3	1.38	2.43	6.0	1.56	2.10	8.7	4.55	5.57
3.4	1.29	2.40	6.1	1.59	2.13	8.8	4.30	5.19
3.5	1.35	2.49	6.2	1.57	2.10	8.9	4.02	4.83
3.6	1.52	2.67	6.3	1.51	2.03	9.0	3.77	4.48

Table 12 Distributions of gamma-ray exposure dose in the access way measured by UD-200S TLD

Distance from Duct Inlet (cm)	Exposure Dose Rate (mR hr^{-1}/source neutron sec^{-1})				
	A-line			B-line	C-line
	*100cm	*180cm	*20cm		
-100	1.91(±0.1)-09**			1.95(±0.15)-09	2.00(±0.15)-09
- 50	1.80(±0.1)-09				
0	1.61(±0.1)-09	1.60(±0.1)-09	1.52(±0.1)-09	1.54(±0.15)-09	1.73(±0.15)-09
50	7.41(±0.4)-10				
100	3.91(±0.2)-10			4.02(±0.30)-10	3.11(±0.30)-10
150	2.35(±0.15)-10				
200	1.58(±0.12)-10	1.32(±0.12)-10	1.41(±0.12)-10	1.34(±0.15)-10	1.35(±0.15)-10
256	1.07(±0.1)-10	9.81(±1.0)-11	9.84(±1.0)-11		
294				2.16(±0.50)-11	
296					9.37(±1.80)-11
316	7.96(±1.0)-11	6.56(±1.0)-11	6.58(±1.0)-11		
366	3.00(±0.7)-11				
372				7.82(±4.0)-12	
384					7.25(±1.2)-11
416	1.97(±0.7)-11				
460	9.54(±4.0)-12	7.25(±4.0)-12	9.92(±4.0)-12		
462					2.31(±1.0)-11
515	5.53(±2.5)-12				
540					9.73(±4.7)-12
A^- 565	5.92(±1.6)-12				
A^+ 565	4.96(±2.2)-12				
A^- 615	2.86(±1.2)-12				
A^+ 615	3.44(±1.6)-12				

* Detector height

** Read as $1.91(\pm0.1) \times 10^{-9}$

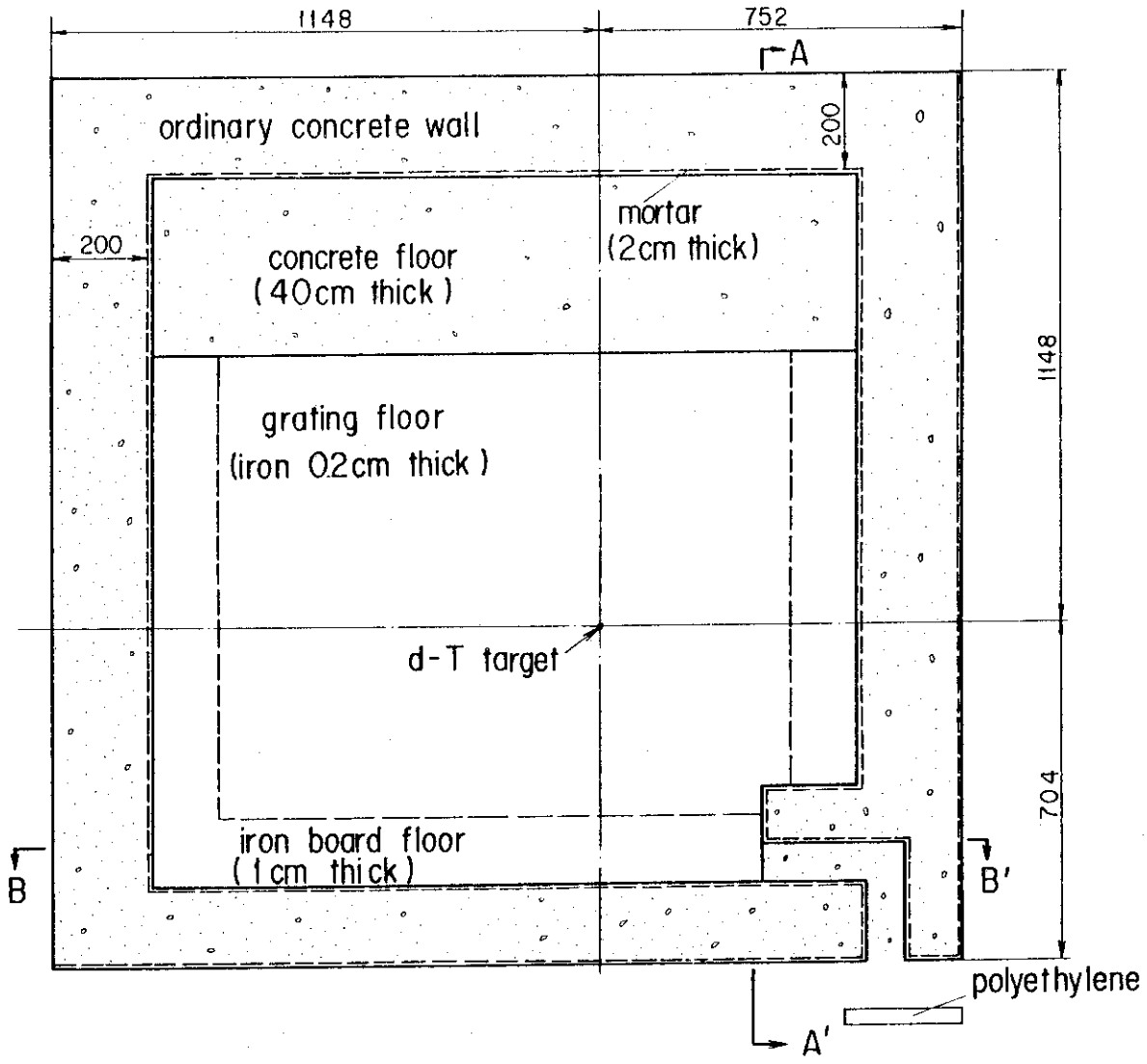

Fig.1 A horizontan view of the 1st target room used for the streaming experiment

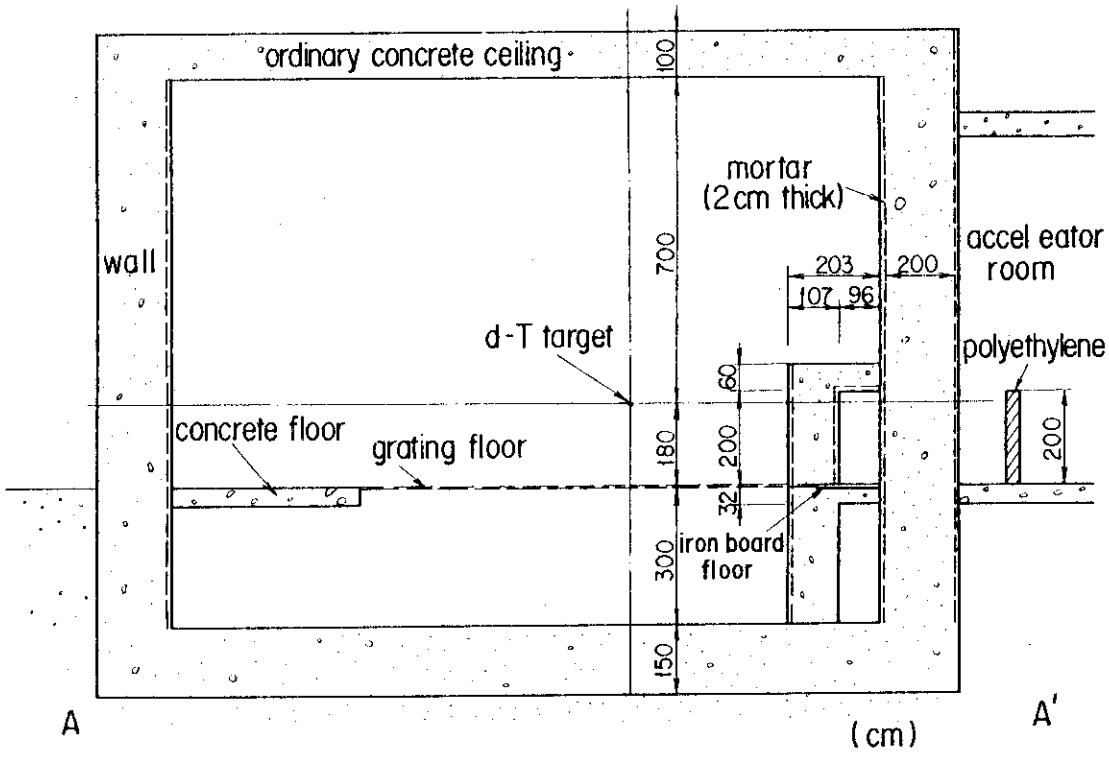

Fig.2 A vertical plan at the AA' cross section shown in Fig.1

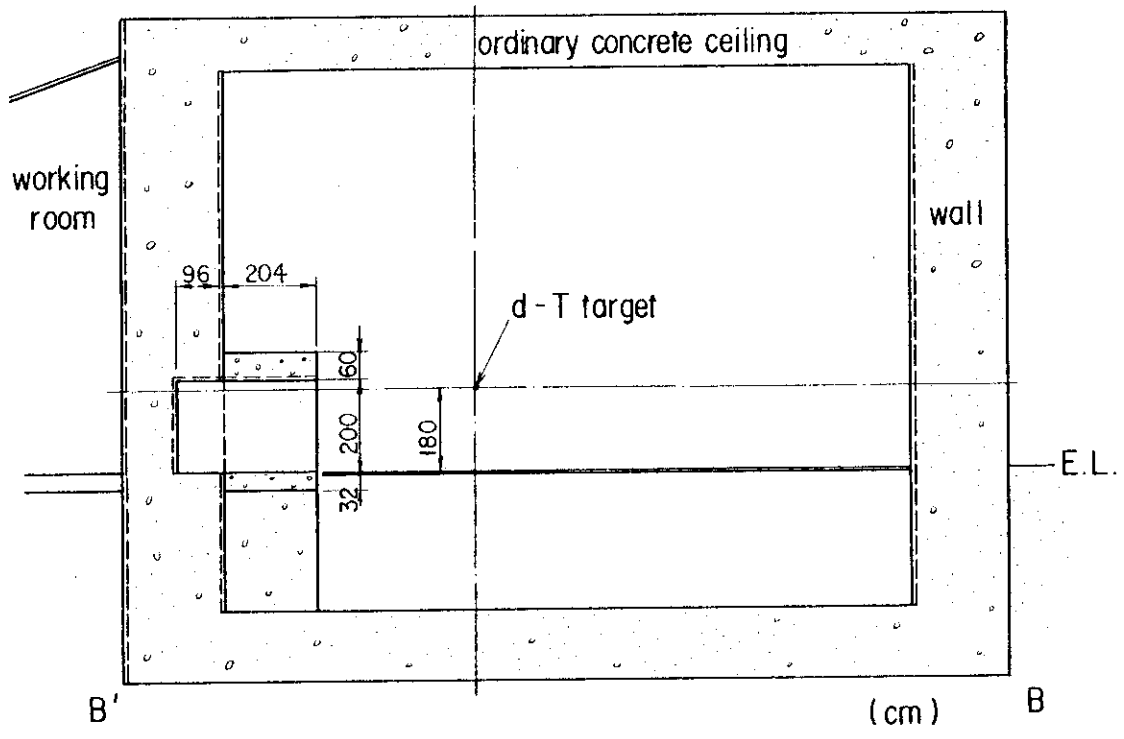

Fig.3 A vertical plan at the BB' cross section shown in Fig.1

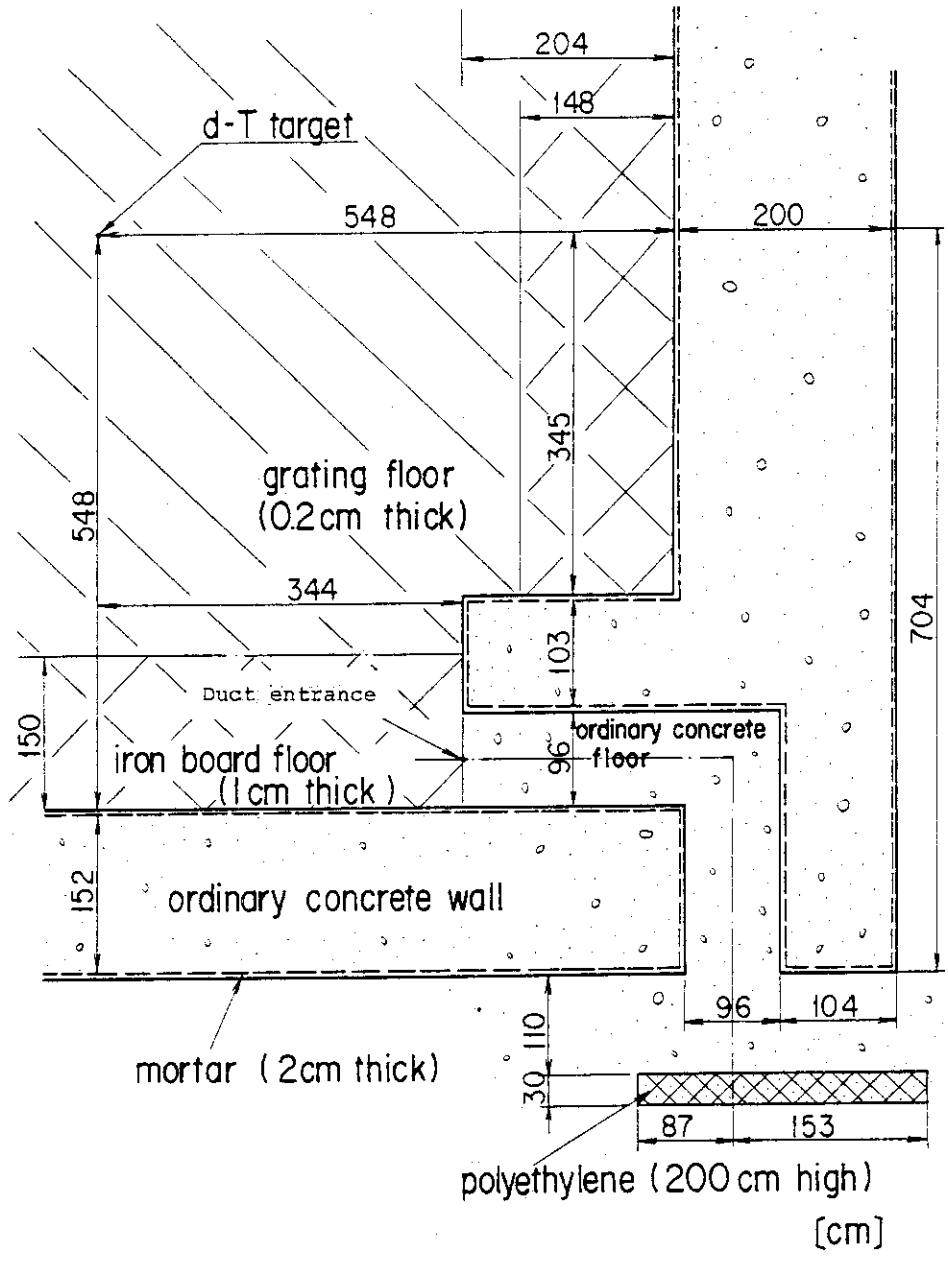

Fig.4 A detail floor plan around the personnel access way

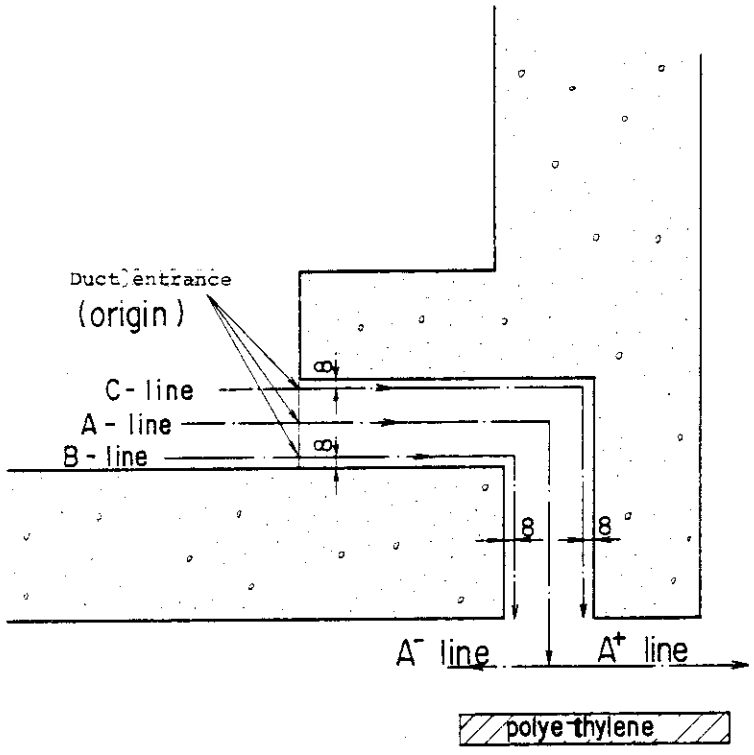

Fig.5 Measured lines in the access way for expriments

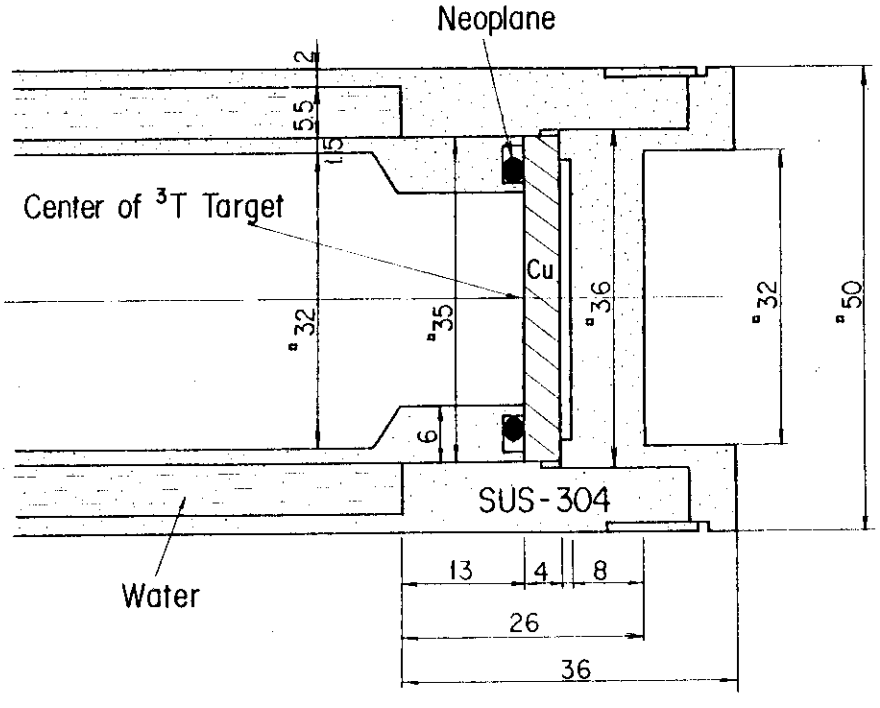

Fig.6 A water-cooled type tritium target assembly

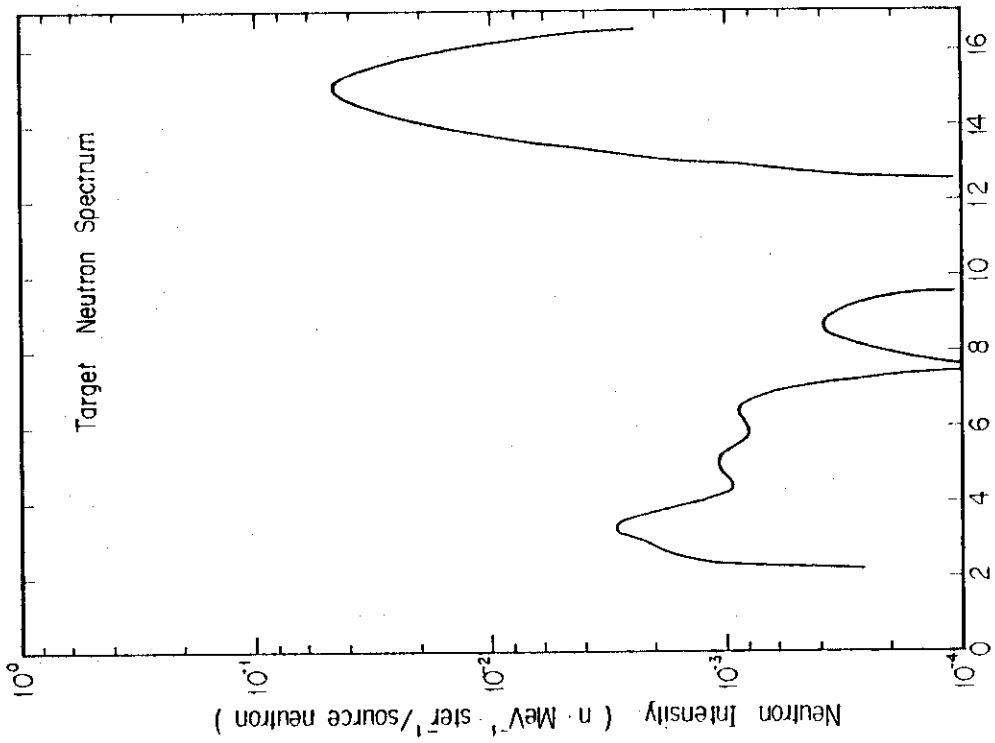

Fig.7 Energy spectrum of the source neutrons from the tritium target to the direction of θ=0°

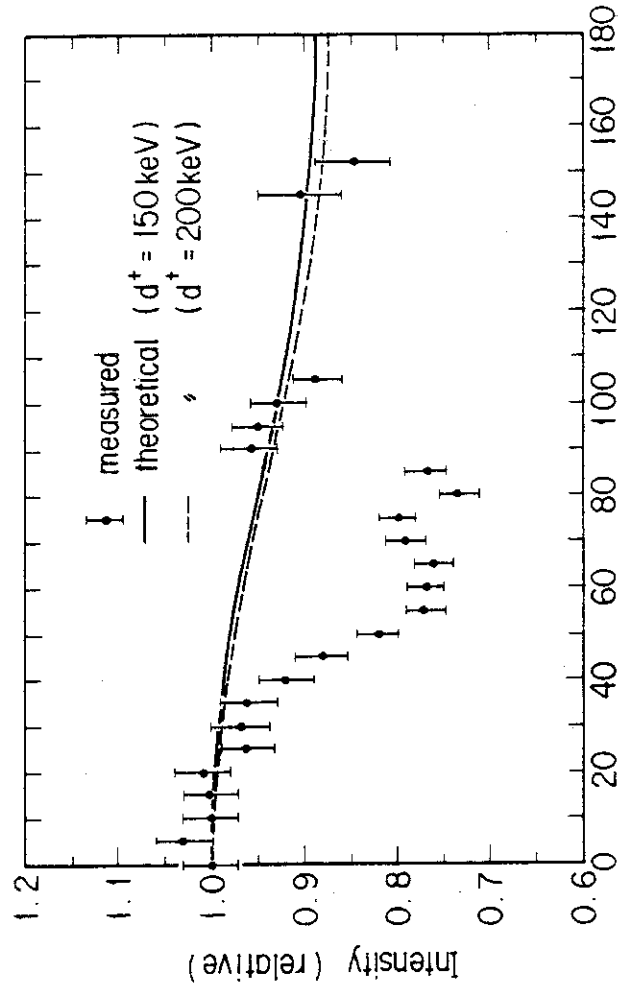

Fig.8 Angular distribution of neutron intensity emitted from the tritium target

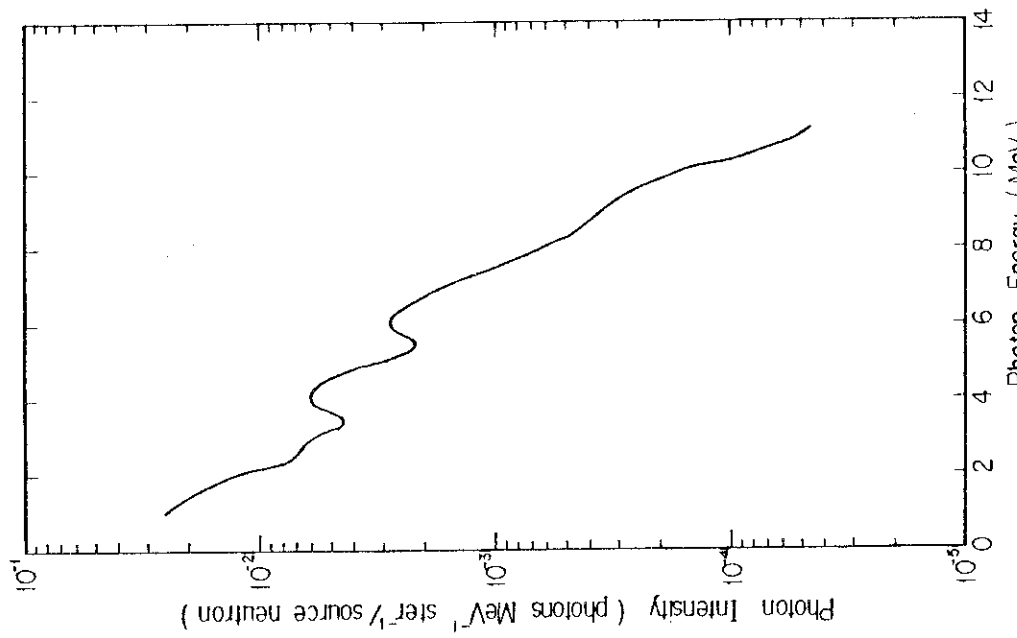

Fig.10 Energy spectrum of the source gamma rays emitted from the tritium target assembly to the direction of θ=90°

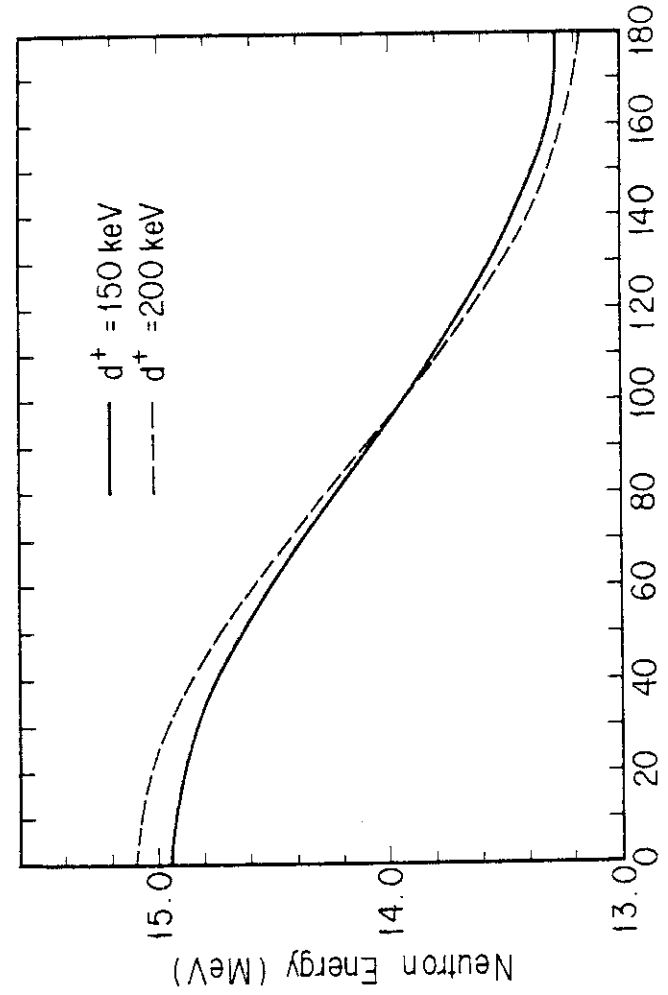

Fig.9 Theoretical angular distribution of D-T neutron energies for the deuteron energy of 150 keV and 200 keV

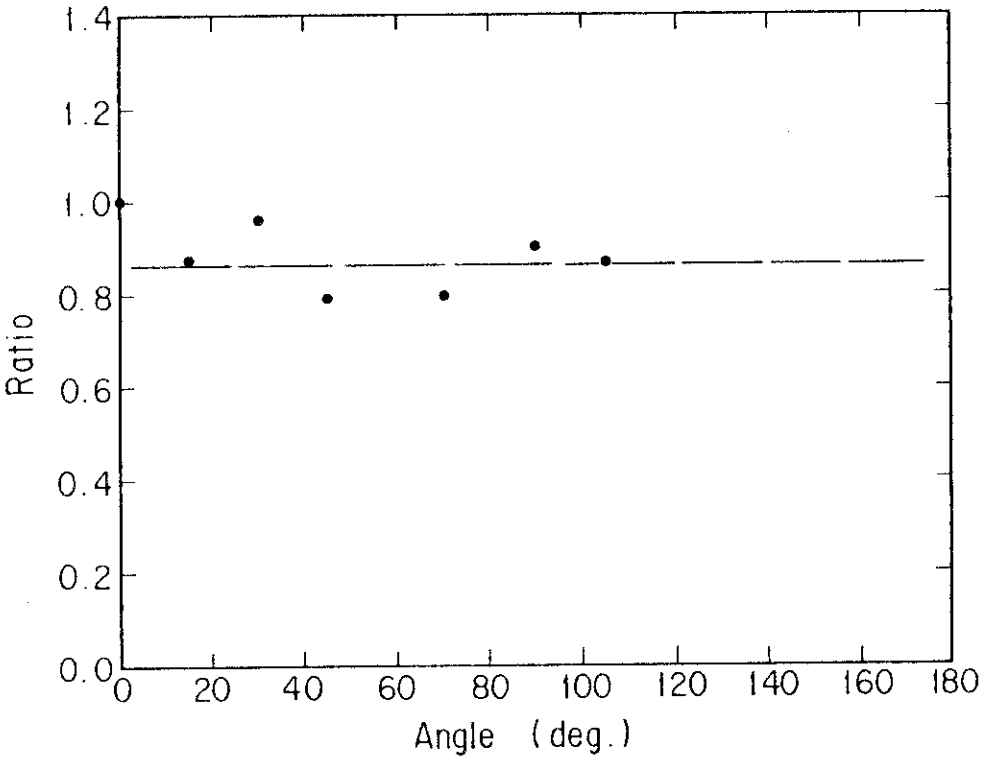

Fig.11 Angular distribution of gamma-ray intensity emitted from the target assembly

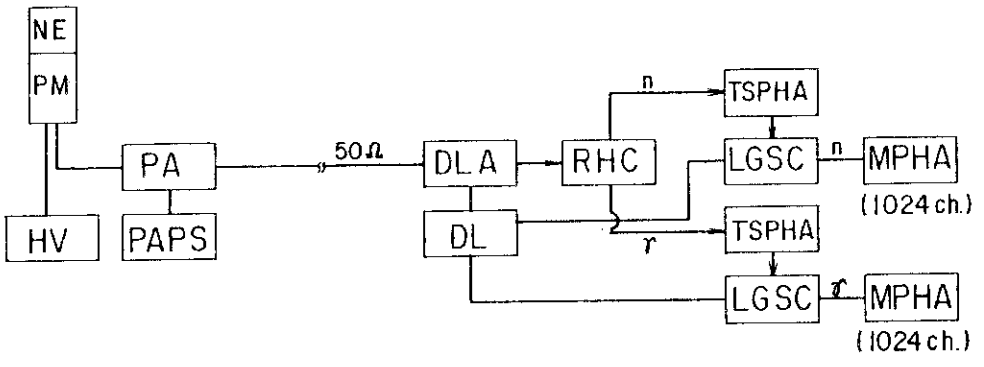

NE : 2"ϕ x 2"t NE213 Liquid Scintillator
PM : Photomultiplier (RCA 6810A)
HV : High Voltage Power Supply
PA : Pre-amplifier
PAPS : Pre-amp Power Supply
DLA : Delay Line Amplifier (ORTEC 460)
DL : Delay Line
RHC : Risetime to Height Converter (JAERI 154A)
TSPHA : Timing Single Channel Pulse Height Analyzer
LGSC : Linear Gate and Slow Coincidence
MPHA : Multi-Channel Pulse Height Analyzer

Fig.12 Block diagram of NE213 detector system for neutron and gamma-ray spectra measurements

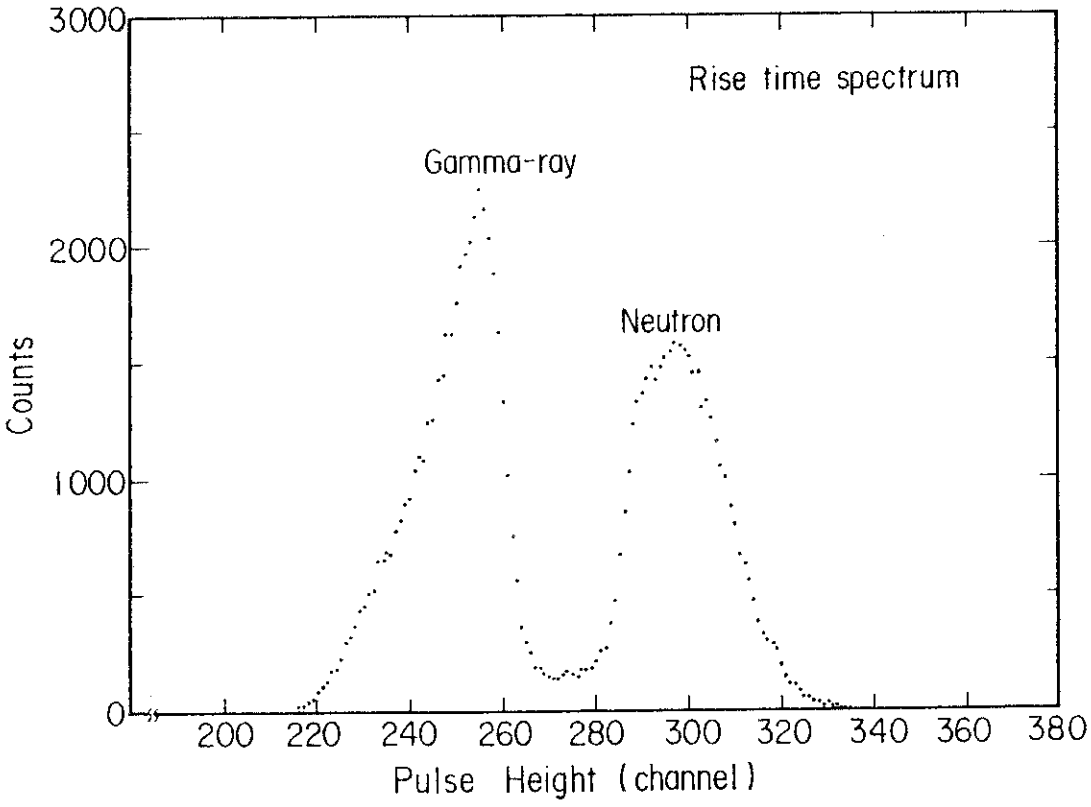

Fig.13 A typical rise time spectrum to neutron and gamma-ray mixed radiations measured using a RHC circuit

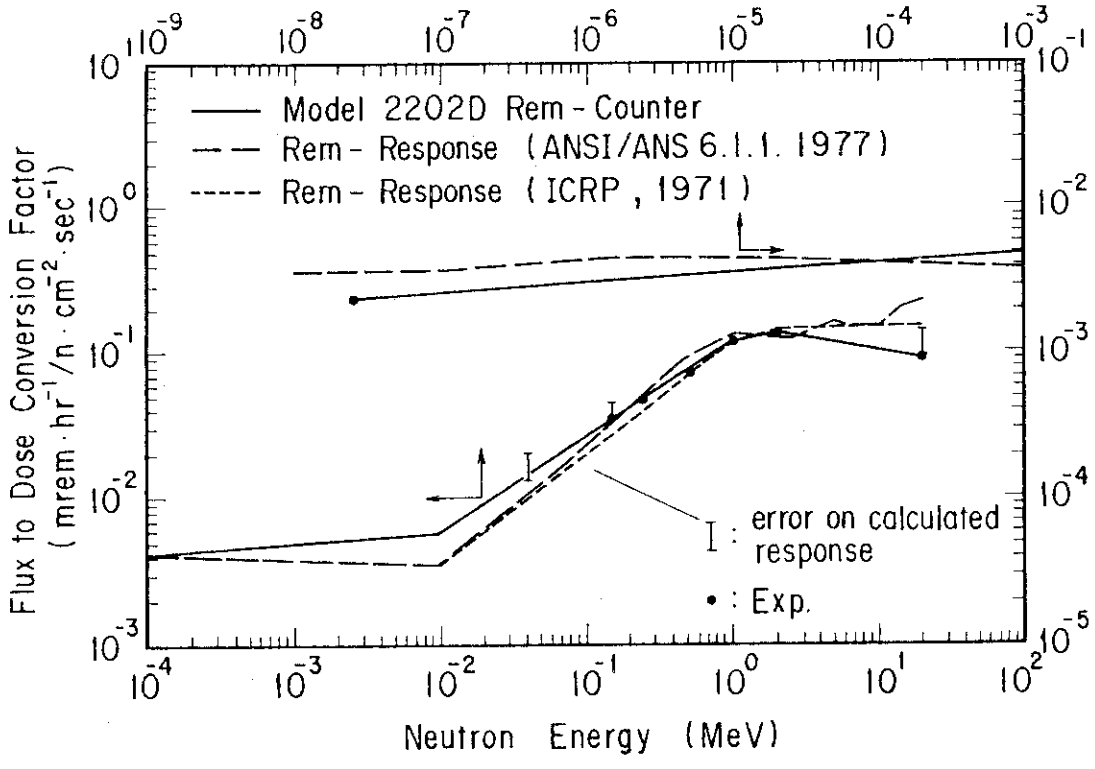

Fig.14 Comparison between the neutron flux to dose conversion factors recommended by ICRP and ANSI/ANS and the neutron response of a Studsvik 2202D neutron dosimeter

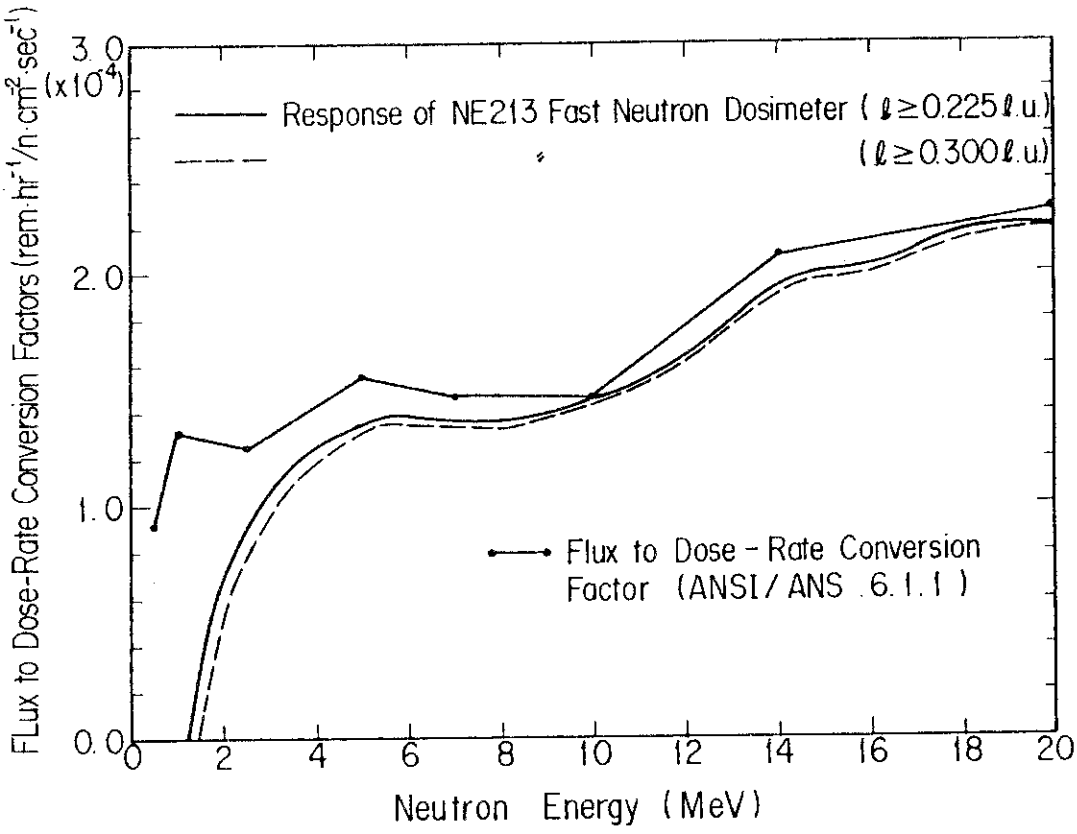

Fig.15 Comparison between the neutron flux to dose conversion factor of ANSI/ANS recommendation and the spectrum weighting functions used for the fast neutron dose measurement

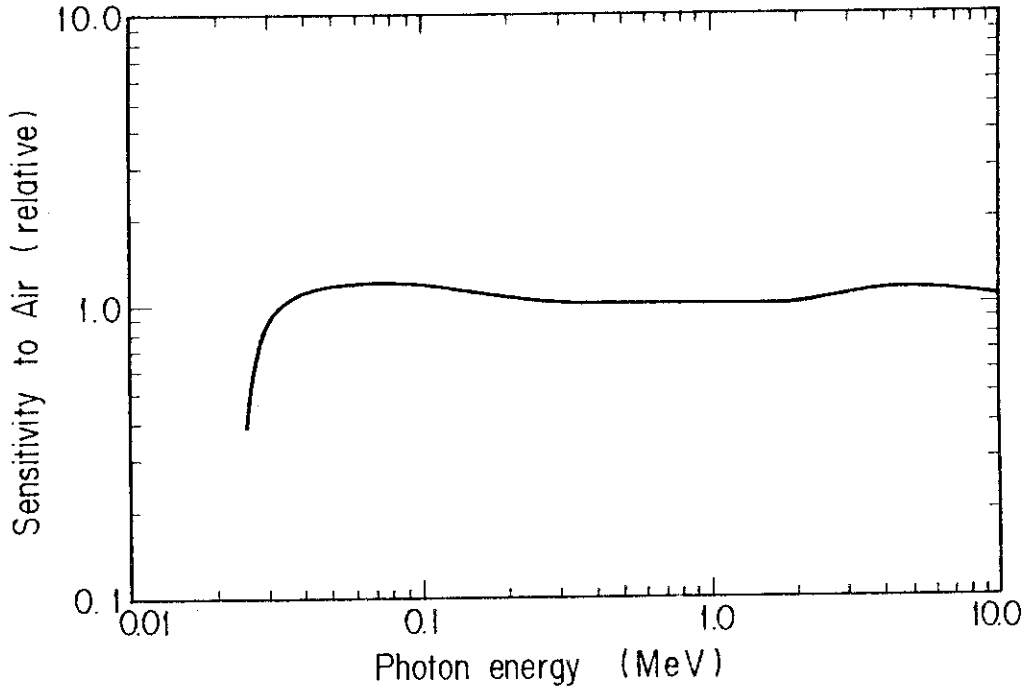

Fig.16 Energy response of $CaSO_4$(Tm) with a gamma-ray filter (UD-200S) TLD to gamma rays, where is normalized to that of air

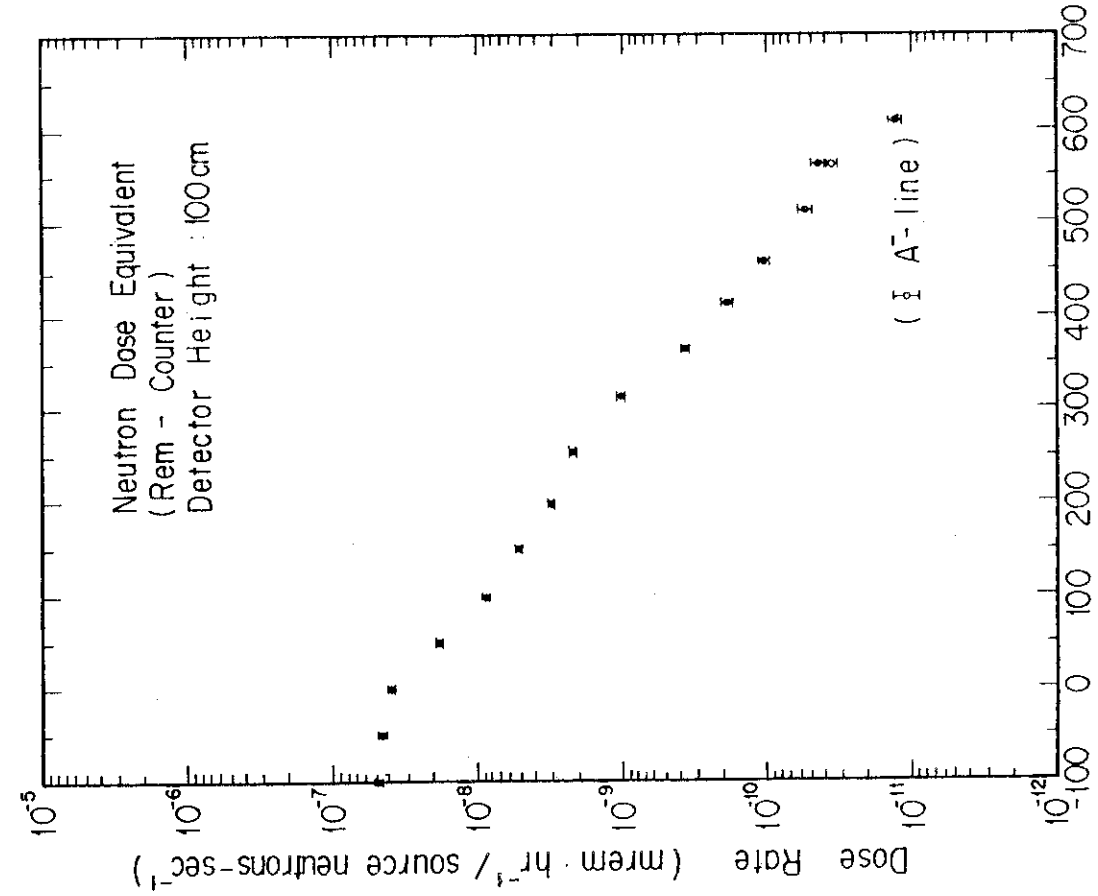

Fig.18 Distribution of neutron dose equivalent in the access way measured by a rem counter

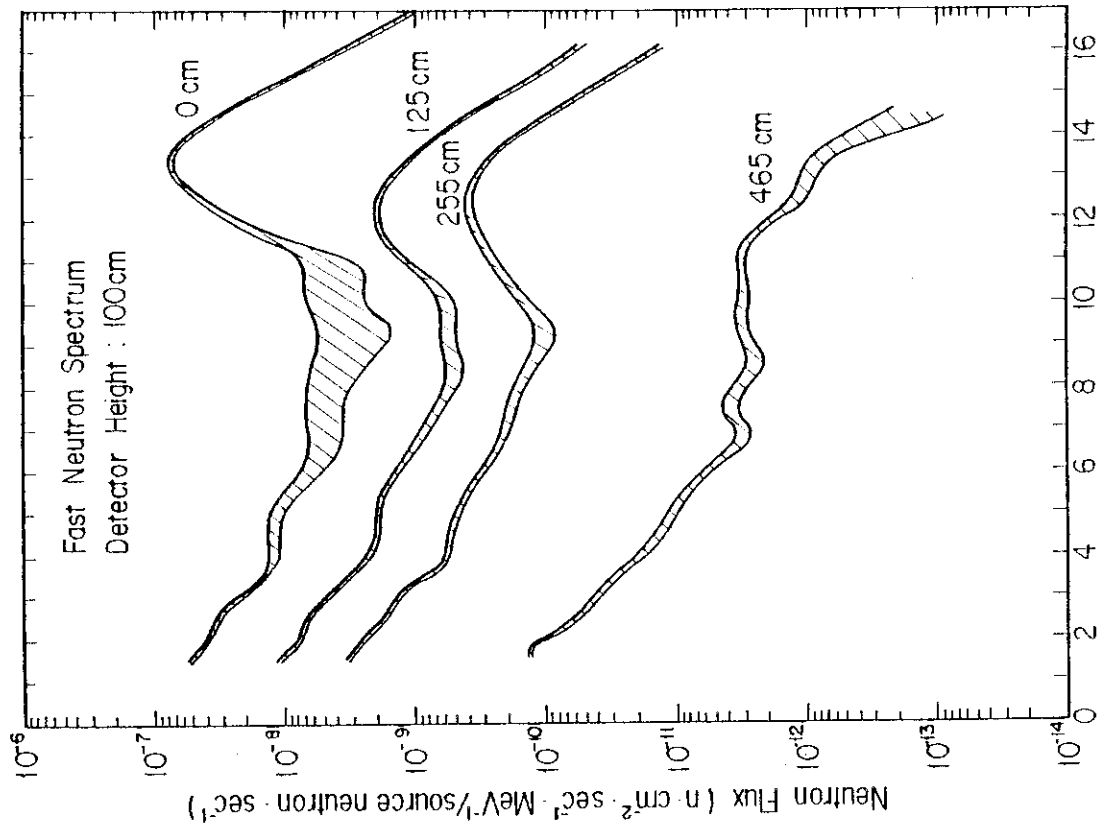

Fig.17 Neutron enerty spectra in the duct measured by NE213 detector

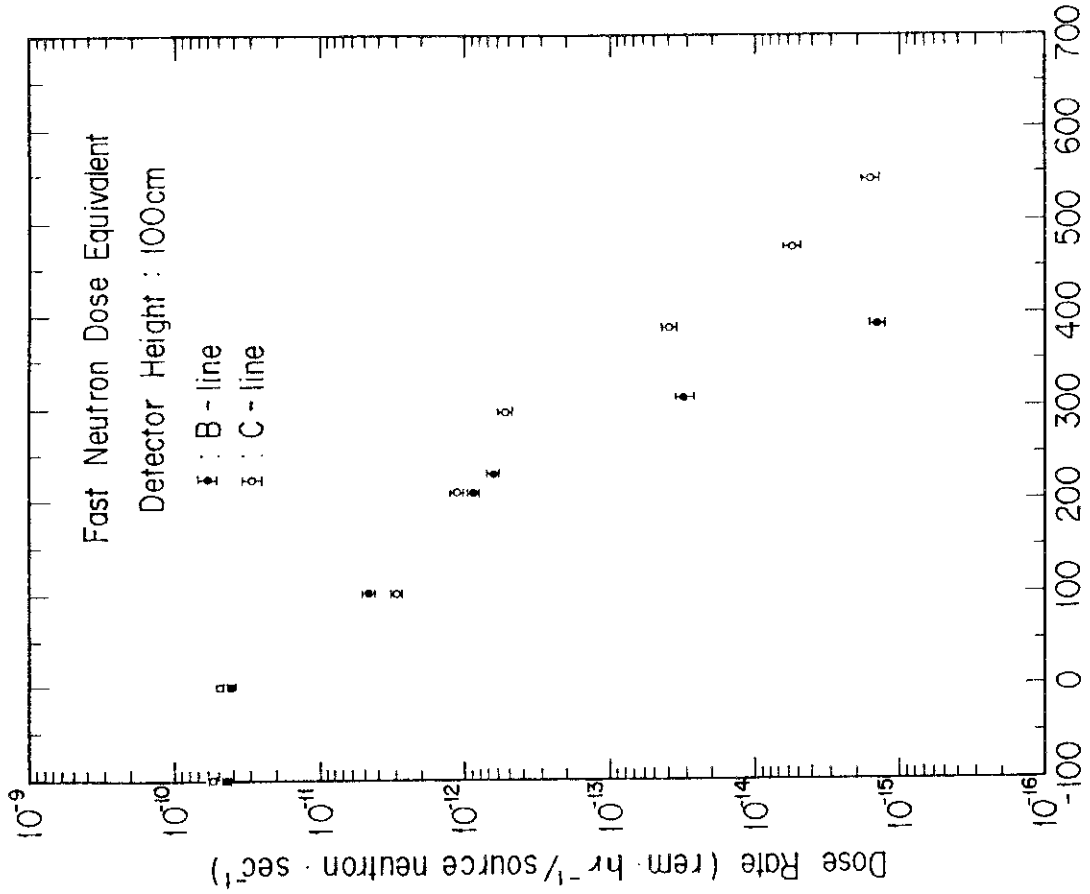

Fig.20 Distributions of fast neutron dose along the B- and C-lines at the height of 100 cm

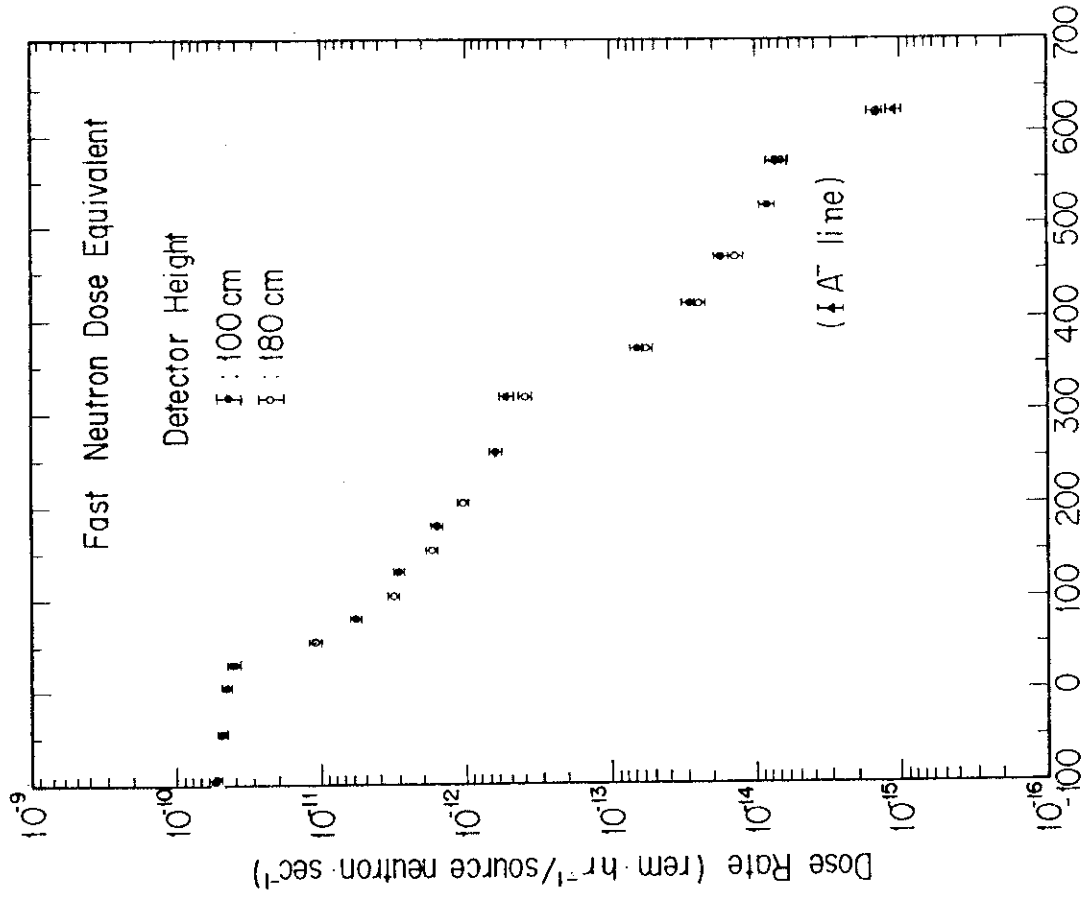

Fig.19 Distributions of fast neutron dose along the A-line at the height of 100 cm and 180 cm

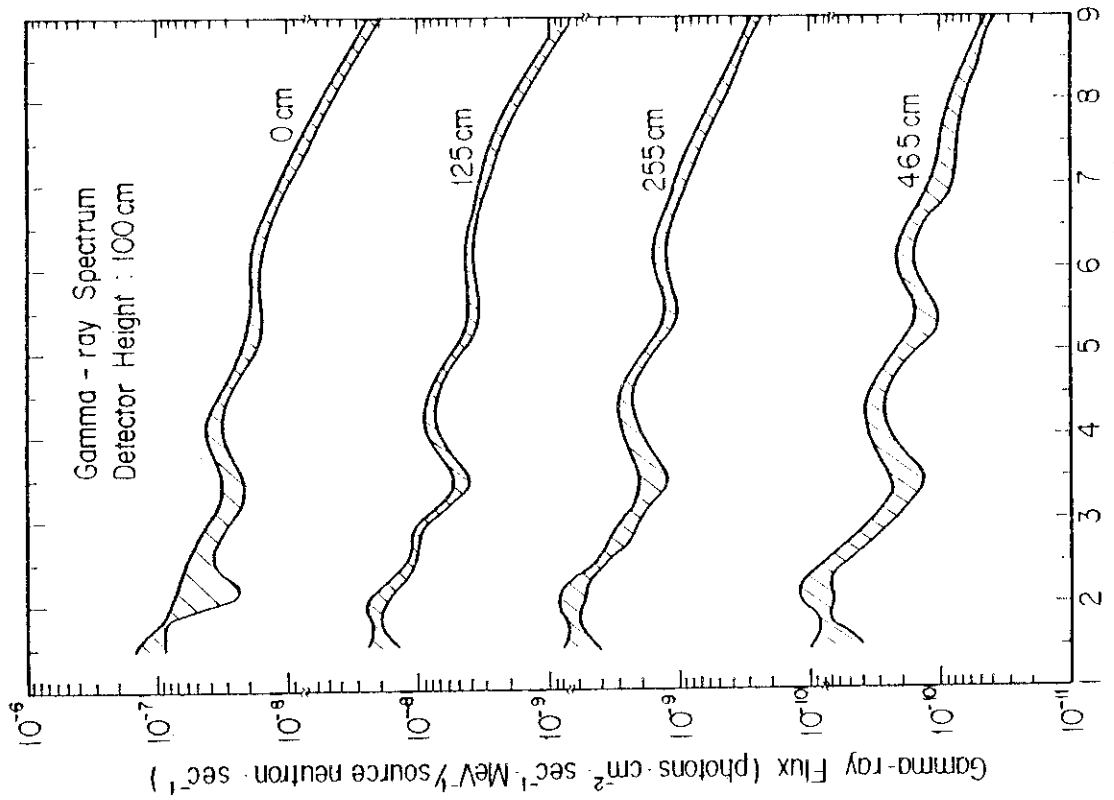

Fig.22 Gamma-ray energy spectra in the access way measured by NE213 detector

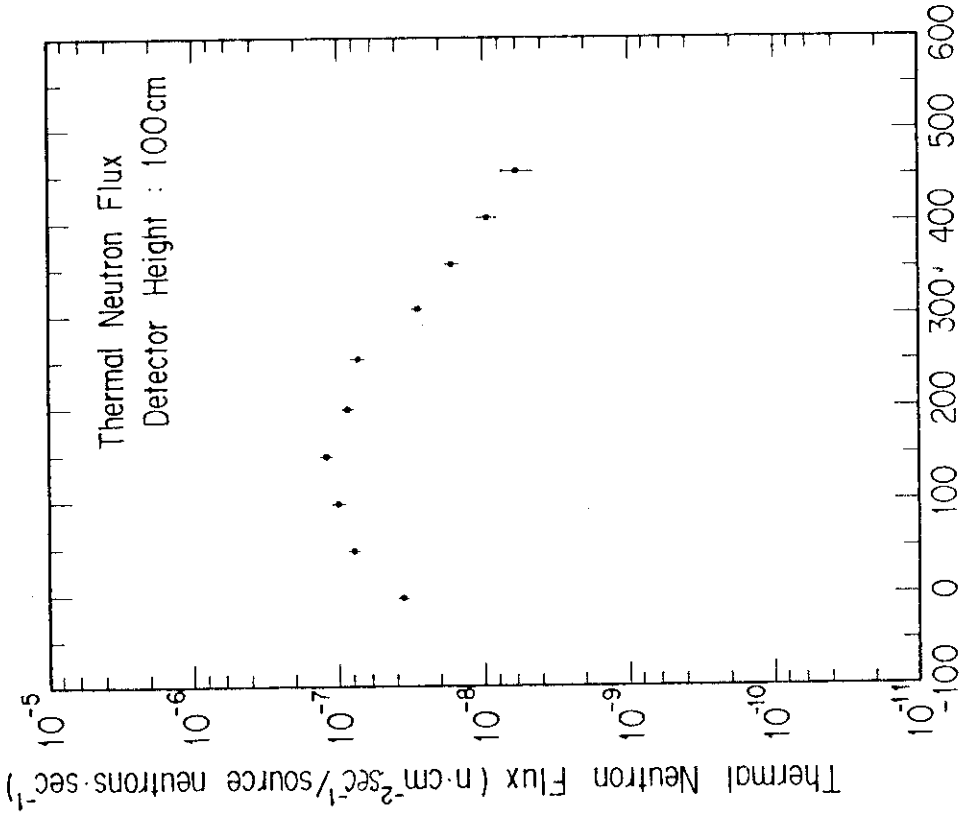

Fig.21 Distribution of thermal neutron flux along the A-line at the height of 100 cm

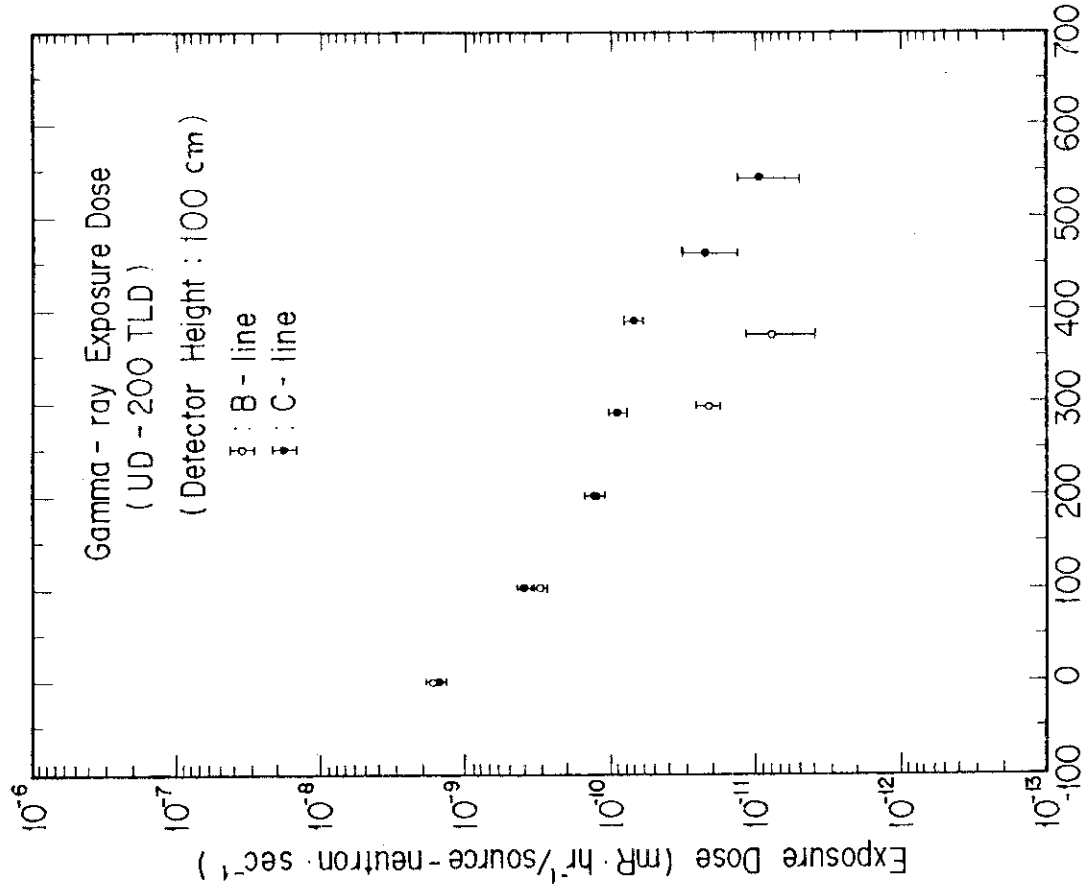

Fig.24 Distributions of gamma-ray exposure dose along the B- and C-lines at the height of 100 cm

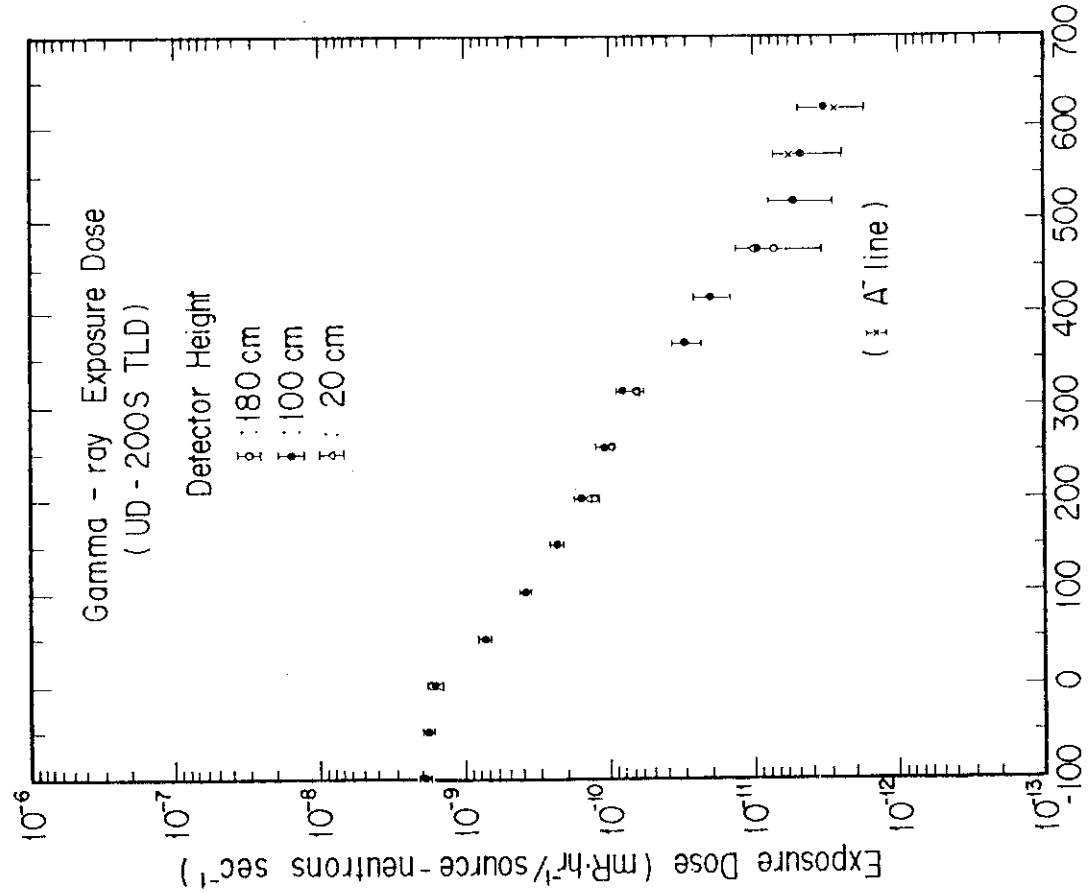

Fig.23 Distributions of gamma-ray exposure dose along the A-line at the height of 20 cm, 100 cm and 180 cm